AD-A035 378 TEXAS UNIV AT AUSTIN ELECTRONICS RESEARCH CENTER F/G 9/4
MULTICHANNEL IMAGE DECODING,(U)
JAN 76 J KNOPP, E L HIXSON F44620-71-C-0091
UNCLASSIFIED TR-178 AFOSR-TR-77-0009 NL

1 OF 2
AD-A
035378

MULTICHANNEL IMAGE DECODING

TEXAS UNIVERSITY AT AUSTIN
AUSTIN, TEXAS

15 JANUARY 1976

MULTICHANNEL IMAGE DECODING

by

Jerome Knopp and Elmer L. Hixson

Department of Electrical Engineering

Technical Report No. 178

January 15, 1976

ACOUSTICS RESEARCH LABORATORY

ELECTRONICS RESEARCH CENTER
THE UNIVERSITY OF TEXAS AT AUSTIN
Austin, Texas 78712

The Electronics Research Center at The University of Texas at Austin constitutes interdisciplinary laboratories in which graduate faculty members and graduate candidates from numerous academic disciplines conduct research.

Research conducted for this technical report was supported in part by the Department of Defense's JOINT SERVICES ELECTRONICS PROGRAM (U.S. Army, U.S. Navy, and the U.S. Air Force) through the Research Contract AFOSR F44620-71-C-0091. This program is monitored by the Department of Defense's JSEP Technical Advisory Committee consisting of representatives from the U.S. Army Electronics Command, U.S. Army Research Office, Office of Naval Research, and the U.S. Air Force Office of Scientific Research.

Additional support of specific projects by other Federal Agencies, Foundations, and The University of Texas at Austin is acknowledged in footnotes to the appropriate sections.

MULTICHANNEL IMAGE DECODING*

by

Jerome Knopp and Elmer L. Hixson
Department of Electrical Engineering

Technical Report No. 178
January 15, 1976

ACOUSTICS AND RADIO SCIENCES LABORATORY

ELECTRONICS RESEARCH CENTER
THE UNIVERSITY OF TEXAS AT AUSTIN
Austin, Texas 78712

*Research Sponsored by the Joint Services Electronics Program under Research Contract F44620-71-C-0091

ABSTRACT

Multichannel image decoding is a very general scheme to improve the signal-to-noise ratio in decoding images coded with linear shift invariant codes. It is shown that it can be advantageous to code an image with more than one code. A "composite" inverse filter can then be used in the frequency plane to recover the Fourier transform of the original image. To recover a particular point in the frequency plane, the inverse filter for any one of the coded versions of the image, that is any channel, can be used. The channel with the highest signal-to-noise ratio is used to recover the desired point. A particular application of this scheme is examined. A two-channel code is compared with a one-channel code in the frequency domain for the case of misfocus blurring. A graphical analysis is given which compares the distance in the frequency plane up to the first zero in the restored transfer function for one- and two-channel deblurring.

Binary plots of the restored transfer functions for a dynamic range of 100 are shown for the two different coding schemes. These plots show that the two-channel code recovers 37% more area in the frequency plane than the one-channel code. This increased area restores information missing near zeros in the one-channel transfer function. An optical simulation was made using the binary plots as frequency plane filters. Using photographs of subjects with a significant amount of line and edge structure, it is shown that the two-channel code results in "sharper" decoded images.

TABLE OF CONTENTS

TABLE OF CONTENTS
(Continued)

LIST OF FIGURES

LIST OF FIGURES
(Continued)

LIST OF FIGURES

CHAPTER 1

INTRODUCTION

It is the purpose of this chapter to define the coded image in terms of a linear mapping. The particular case of an image coded with a linear shift invariant mapping will be discussed. A brief review of past research on coding and decoding is included. The recent research on inverse filtering will be of special interest in Chapter 3. The scope of this report and its important contributions are summarized at the end of this chapter.

1.1 THE LINEAR SPACE INVARIANT CODE

Consider the situation shown in Fig. 1. A planar radiant object lies in the $x_1 - y_1$ plane. The intensity distribution $s(x_1, y_1)$ is mapped by some arbitrary image coding system into the $x_2 - y_2$ plane. At this plane a coded image $g(x_2, y_2)$ is formed. The image coding system is similar to the "black box" used in linear circuit analysis, where s

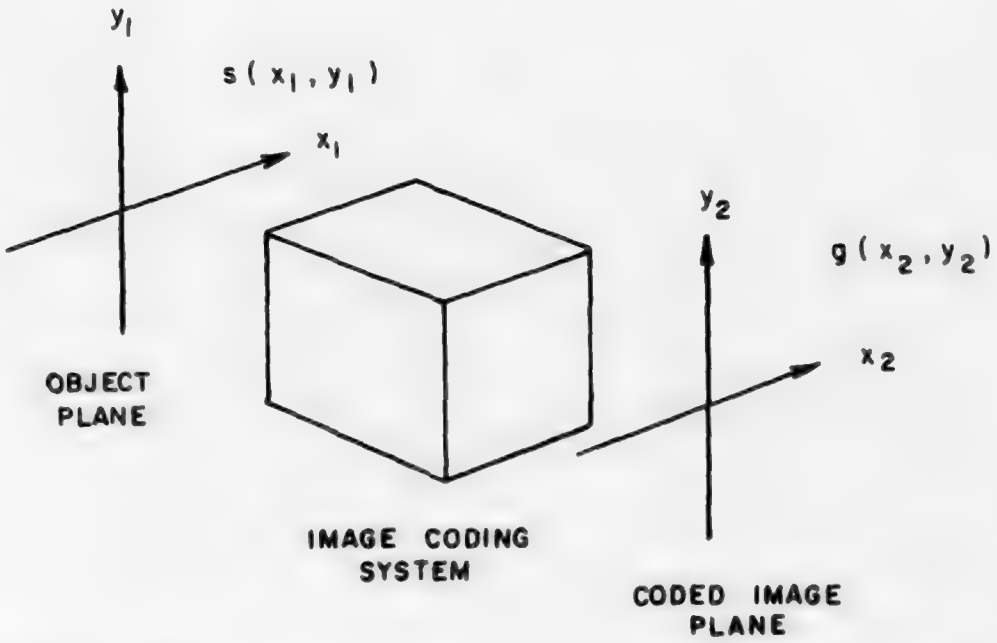

Figure 1. The Original Encoded Image Intensity $s(x_1, y_1)$ is Mapped into the Coded Image Intensity $g(x_1, y_1)$ by Some Arbitrary Image Coding System.

and g represent the input and output of the box respectively. This coding system could, for example, physically refer to some arrangement of lenses and apertures or some random process such as an optically turbulent atmosphere through which a coded image $g(x_2, y_2)$ is obtained. This coded image is usually blurred or distorted and its intensity distribution differs from $s(x_1, y_1)$. In a very general case the mapping from s to g may be described by[1]

$$g(x_2, y_2) = \int_{-\infty}^{+\infty}\int h\left[x_1, y_1\ x_2, y_2,\ s(x_1, y_1)\right] dx_1\, dy_1 \quad . \quad (1-1)$$

Here the function h is called the "impulse response". Equation (1 - 1) describes a very arbitrary nonlinear mapping. Fortunately in many important cases the mapping is considerably simpler in practice. If the impulse response can be used to weight the object distribution and the coded image can be represented as a weighted sum (or integral in the continuous case) over $s(x_1, y_1)$, then the following relation exists between $g(x_1, y_1)$ and $s(x_2, y_2)$:

$$g(x_2, y_2) = \int_{-\infty}^{\infty}\int h\,(x_1, y_1,\ x_2, y_2)\ s\,(x_1, y_1)\ dx_1\, dy_1 \quad (1-2)$$

Equation (1 - 2) represents a linear mapping between s and g. The intensity distribution $g(x_2, y_2)$ is the superposition of the impulse response from every point of $s(x_1, y_1)$. However, even the relationship described in (1 - 2) is quite complicated, and in many cases of practical interest an additional simplification can be made:

$$h(x_1, y_1, x_2, y_2) = h(x_2 - x_1, y_2 - y_1). \qquad (1 - 3)$$

In this case the system is said to be space-invariant. This is analogous to time invariance associated with linear circuit analysis. Equation (1 - 3) assumes that translating the input intensity distribution s causes the output g to be translated in direct proportion. It will be assumed in what follows that only linear space invariant systems will be used in coding.

1.2 THE TWO-DIMENSIONAL FOURIER TRANSFORM

The linear space-invariant optical system like time-invariant electrical systems is easy to discuss in the Fourier transform domain. To handle two-dimensional variables, a two-dimensional Fourier transform is used. (This can be

derived directly from the definition of a one-dimensional transform.[2]) The two-dimensional Fourier transform pair associated with the function $g(x,y)$ is $F(g)$ where

$$F(g) = \int_{-\infty}^{+\infty}\int g(x,y)\, \exp\left[-j\,2\pi\,(x\xi + y\eta)\right]\, dx\,dy \quad . \qquad (1-4)$$

Here, the expression "exp (ω)" is used for e^{ω}. The Fourier transform $F(g)$ is the function $G(\xi, \eta)$, where ξ and η are rectangular coordinates in the frequency domain and are referred to as frequency variables or simply frequencies. Either g or G can be used as an adequate description of an intensity distribution. The intensity distribution is represented by either function; $g(x,y)$ is referred to as the space domain description. Given the frequency domain description $G(\xi, \eta)$, then $g(x,y)$ can be found in the space domain using the two-dimensional inverse Fourier transform:

$$g(x,y) = \int_{-\infty}^{+\infty}\int G(\xi, \eta)\, \exp\left[\, j\,2\pi\,(x\xi + y\eta)\right] d\xi\, d\eta \quad . \qquad (1-5)$$

The function g must satisfy Dirichlet conditions for Eqs. (1 - 4) and (1 - 5) to be meaningful. However, if a function is physically possible, this is a sufficient condition.[3] The problem

in using the definitions given in (1 - 4) and (1 - 5) usually occurs when the physical situation is only approximately modeled using idealizations such as the Dirac δ function. These situations usually require an interpretation in terms of generalized functions. These pathological anomalies will be ignored in discussions which follow, and instead the reader is referred to works including a more advanced discussion.[4,5] Results from Fourier analysis will be used freely without going into proofs of theorems.

One of the most useful theorems in respect to linear system theory is the convolution theorem. If the convolution of two functions s and h is g, then

$$g(x,y) = \int_{-\infty}^{+\infty}\int s(x,y)\, h(x'-x,\, y'-y)\, dx'\, dy'. \qquad (1-6)$$

This may be written in a more compact notation using an asterick to indicate convolution:

$$g = s * h \quad . \qquad (1-7)$$

Note that the convolution integral (1 - 6) is equivalent to a linear space-invariant mapping of s to g. The convolution

theorem states that this mapping may be described as a product in the frequency domain:

$$G = H S \ . \qquad (1 - 7)$$

The upper-case variables G, H, and S represent the Fourier transforms of the lower-case variables g, h, and s, respectively. In Eq. (1 - 7), H is referred to as the transfer function. If the mapping from s to g is a coding operation, then H is called the "coding" transfer function. The relationship between Eqs. (1 - 6) and (1 - 7) will prove quite useful later when the decoding process is discussed.

1.3 PAST RESEARCH ON CODING AND DECODING

In this section, coding and decoding will be put in its historical perspective. The brief review given here covers coding from a more general viewpoint. It should, however, give a good idea of the relationship of the main topic of this report to previous research.

1.3.1 Bragg Imaging, Holography, and Crystallography

Historically the earliest attempts using a coding-

decoding process was one used by Bragg[6,7]. As early as 1929 he produced images of crystal structure. Bragg was able to obtain the amplitude of Fraunhoefer patterns from X-ray diffraction data. The Fraunhoefer pattern is equivalent to the Fourier transform of the atomic diffracting structure. This may be viewed as a coded version of the image structure. The image was recovered by taking another Fourier transform of the coded image to recover a decoded image. This second transform was accomplished using diffraction in the visible region in coherent light to view the atomic structure. A similar idea involving a double diffraction system will be used in Chapter 3 to carry out some optical computations. Bragg's imaging process required that the phase of the recorded transform be known. In 1948 Gabor[8,9] introduced a similar coding scheme that recorded phase as well as amplitude of a diffracted field using coherent radiation. In this process the amplitude and phase are coded in the form of an intricate diffraction grating. This grating, called a hologram, is made from the interference pattern between the original object wave and a reference wave.

The interference pattern is recorded on a photographic emulsion. The object is decoded by viewing the diffracted wave from the hologram.

Other methods using incoherent light for coding have been used in crystallography to record Patterson projections of atomic structure.[10] Such projections can be interpreted as coded versions of atomic structure. These patterns are used as models and are created using convolutions or correlations in visible incoherent light. The Patterson projections can be compared with X-ray diffraction patterns and aid in estimating the crystal structure.

1.3.2 Zone Plate Imaging and Aperture Coded Imaging

The recorded diffraction pattern in Gabor's holography was interpreted in terms of a generalized zone plate by Rogers.[11,12] This interpretation led Mertz and Young[13,14] to the earliest aperture coding scheme, zone plate imaging. In zone plate imaging, the object to be coded was placed in front of a zone plate aperture as shown in Fig. 2. Each point on the object creates its own scaled shadow or projection of

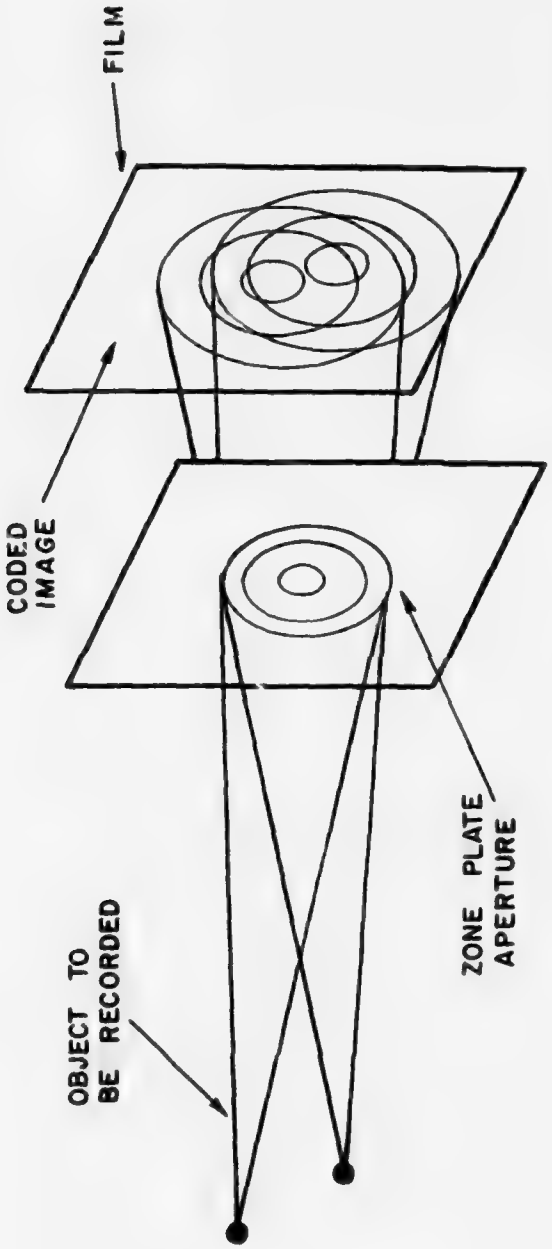

Figure 2. Aperture Coding of Two Points by Shadow-Casting with a Zone Plate.

the zone plate aperture at the recording plane on photographic film. This is shown in Fig. 2 for a two-point object. For an object with a continuous intensity distribution, the coded image is a convolution of the object with a zone plate. Aperture coded imaging may be described by the integral in Eq. (1 - 6) if the object being coded is planar. In this case, the impulse response is essentially a space invariant zone plate. This plan works well, provided the laws of geometric optics hold and diffraction (see Chapter 2) is negligible. When this is not the case, then the "diffracted" projection of a single point must be used for the impulse response. When geometric optics does hold the coding is similar to holography. The diffraction from the coded image is used to decode the coded image in a manner similar to a Gabor hologram. Recently this technique has been revived for gamma ray imaging.[15,16,17]

Dicke[18] has proposed a more general aperture for coding and decoding. In his scheme a random array of pinholes has been used as a coding aperture. To decode an image coded with a pinhole array, a positive transparency of the coded image is optically correlated with the original coding mask.

The correlation peaks in this process produce a decoded image. This correlation scheme has been tested and was shown feasible for Gamma ray and X-ray imaging of stars.[19] In this case the correlation was carried out using holography. Weiss[20] has recently improved the correlative technique using spatially incoherent light and a non-redundant array of points suggested by Golay's[21] work. In addition, optical correlation in totally incoherent light has been used in decoding.[22]

1.3.3 Deblurring and Image Restoration

In 1953 Marechal[23] and co-workers had experimented with a double diffraction arrangement to carry out optical filtering. Marechal's approach involved placing a compensating filter in the frequency domain representation of a defective photographic transparency. The Fourier transform of the defective transparency was calculated optically using a lens and coherent light. (This operation will be described in detail in the next chapter.) The compensating filter was used to reshape the Fourier spectrum to a more desirable one. A second lens was used to calculate the corrected or decoded

image from the corrected transform using a second diffraction process. In Chapter 3 a similar computation system is discussed. Marechal introduced the idea of "inverse" filtering using an optical computer. (Inverse filtering will be discussed in the next section.) In early research the compensating filters were very simple. However, in general such filters are complex two-dimensional functions. These filters must correct phase as well as amplitude and are not easy to construct. Tsujiuchi[24,25] constructed improved deblurring filters for amplitude and phase correction. The process he used in making his filters was very difficult. The phase part of his filters was made by evaporating MgF_2 onto a glass plate and etching out the proper phase correcting filter. Such filters gave good results especially on defocussed blur. Stroke[26,27,28] and co-workers have considerably improved inverse filtering by making the compensating filters holographically. Holographic filters provide phase correction by grating diffraction. Such filters can be made using only photographic processes. Recently Ragnarsson[29] has improved the holographic decoding filter by increasing the dynamic range. This filter is made using a bleached hologram

and results in a filter that is optimum with respect to additive grain noise. Tichenor[30] has recently improved Ragnarsson's filter by eliminating the effect of phase errors inherent in the bleached hologram.

Various types of filtering have also been carried out on the digital computer for image restoration. Many of these techniques are analogous to the optical decoding schemes described above.[31,32,33] However, there are more challenging schemes that can be carried out using the digital computer. The schemes described up to now carry out decoding using "a priori" information. This implies a knowledge of the process used in the coding. It is possible in certain cases to estimate the coding process from the coded image only. This type of decoding uses "a posteriori" information. An example of such a scheme is "blind deconvolution".[34] Here, it is assumed that the coded picture may be divided into contiguous regions with the intensity distributions in each region statistically independent. It is assumed that each region has the same coding transfer function associated with it. Using the logarithm of

the coding transfer function allows the product in Eq. (1 - 7) to be expressed additively. Then the problem of estimating the coding transfer function is reduced to using any one of the many statistical techniques useful for additive noise.

There are many additional techniques available using the digital computer for decoding. They can be found in review articles on image restoration.[1,35,36]

1.4 INVERSE FILTERING

The inverse filtering scheme first suggested by Marechal is of special interest in relation to multichannel filtering. Consider, as in (1 - 7), an object s in the frequency domain coded with a transfer H to produce the coded image G:

$$G = HS$$

If we multiply both sides of the equation by H^{-1}, this yields

$$S = H^{-1}G \quad . \qquad (1 - 9)$$

In principle, S is completely recoverable if H^{-1} is known and the frequency domain multiplication in (1 - 9) can be carried out. This can be done on a digital computer using a sampled version of the coded image g and the fast Fourier transform to obtain

the complex frequency domain representation: G. The sampled coded image can be obtained by optically scanning and digitizing the intensity information from a transparency or photograph of the coded image. Equation (1 - 9) is then executed as a set of complex multiplications. Also, as will be shown later, a transparency of g can be used directly in an optical computer to yield G. This process is used in the inverse filtering schemes discussed in the previous historical section.

Although the ideas above are very appealing, the inverse filtering scheme unfortunately cannot be realized directly in practice, since the function H^{-1} may contain poles and, due to noise limitations in the original coding process, H^{-1} has fixed dynamic range and cannot take on infinite values. In practice, only approximations to H^{-1} are used, usually a least mean square estimator. This will be discussed more in Chapter 3.

1.5 MULTICHANNEL FILTERING

In Chapter 3 a new scheme is suggested that can improve considerably the inverse filter described above.

Multichannel filtering is an "a priori" scheme in which the same object is coded more than once using different codes. The different coded versions of the image are chosen to maximize the signal-to-noise ratio. A related idea has been used in "multiframe analysis" for "posteriori" processing of coded images.[37] It is especially suitable for images degraded by atmosphere turbulance. In this case the object is coded with a set of different codes but it is assumed that the transfer functions associated with the codes are statistically independent. This is the reverse of the "blind deconvolution" technique which uses a single code and multiple images. The "multiframe analysis" can be considered as a special case of the very general scheme of Chapter 3 , where the coding transfer functions are known a priori and are deliberately chosen to optimize the decoding process.

1.6 ADDITIONAL COMMENTS

In the large majority of practical problems, the coded image is usually a degraded image unacceptable for viewing by the human eye. The objective of the decoding

process is to create a decoded image that according to an eye judgment is "better". It should be made clear that decoding does not change the information content of the coded image; it simply shifts the coding format. In fact any physical decoding process must introduce noise and actually lose some information. Decoding is, in a sense, a process where a certain amount of information is lost in exchange for a more convenient interpretation.

1.7 THE SCOPE OF THIS REPORT

In Chapter 2 an introduction to scalar optics is included. This brief review should help in understanding the optical simulation presented later in Chapter 3. Chapter 3 includes the theory of multichannel image decoding with an analysis and optical simulation designed to show its merit in the case of misfocus blurring. Conclusions and suggestions for further research are in Chapter 4.

This report presents the following contributions to image decoding:

(1) A new theory, multichannel image decoding that can be used to improve the signal-to-noise ratio

in inverse filtering.

(2) A graphical analysis that compares one- and two-channel decoding schemes for the case of misfocus blurring.

(3) An optical simulation comparing one- and two-channel decoding that shows considerable improvement in images decoded using a two-channel code.

CHAPTER 2

SCALAR DIFFRACTION THEORY AND FOURIER OPTICS

In Chapter 3 an optical simulation will be carried out using a special arrangement of lenses to carry out an optical computation. In order to understand the workings of this arrangement, some knowledge of scalar diffraction theory and Fourier optics is necessary. It is the purpose of this chapter to provide background in these areas. Scalar diffraction will be described using the concept of the angular spectrum.[38,39,40] This approach is distinctly different from the classical method employing a Greens function solution to the scalar wave equation.[41,42] This presentation, although concise, will be adequate to cover the needs of Chapter 3. For more information on diffraction theory, additional works are listed.[43,44]

2.1 THE ASSUMPTIONS OF SCALAR DIFFRACTION THEORY

The term diffraction refers to any perturbation of a wavefront that is not caused by reflection or refraction.[43] Diffraction phenomena are usually associated with regions where there are discontinuities and variations in the field distribution of electromagnetic radiation. Diffraction is commonly observed in the shadow of a sharp edge where the edge's shadow appears smeared out instead of the sharp light-dark boundary predicted by geometric optics.[41] A very detailed accounting of diffraction requires a vectorial approach. However, it is fortunate that in most practical situations the polarization of the electromagnetic radiation can be ignored and only field amplitudes need be considered. In the discussion which follows, the term "field amplitude" can be used to refer to either the electric field amplitude or the magnetic field amplitude. It will be assumed that only a single vector component of either of these fields is being modeled and that the individual vector components are independent of each other. Actually such components are coupled together, and this coupling must be accounted for

using Maxwell's equations. The model above which uses amplitude only is the basis of "scalar" diffraction theory. Such a theory has been shown to give accurate results experimentally under certain conditions: (1) the size of the diffracting structure must be much greater than a wavelength and (2) the distance from the diffracting structure at which the field is observed is also much greater than a wavelength.[45] These conditions are fulfilled in the experiments which follow. The smallest diffracting structure will be due to macroscopic field modulation caused by variations in the spatial distribution of the average grain density in a photographic emulsion. Due to the limited bandwidth of the emulsion, the smallest size of this structure is on the order of 5×10^{-2} mm. as compared to a wavelength of about 6×10^{-4} mm. The diffracting structure size is limited to the highest spatial frequency in a sinusoidal† grid that can be recorded. Any object that is recorded on film can be

† The sinusoidal grid is a grid whose field amplitude varies sinusoidally in one direction and has no amplitude variation in a perpendicular direction.

considered as a superposition of different sinusoidal grids if the recorded two-dimensional transmittance is decomposed mathematically into its Fourier components. The spatial frequency response of a film is usually expressed in terms of a transfer function whose maximum value is normalized to 1. The absolute magnitude of this transfer function is defined as the modulation transfer function (MTF). The spatial bandwidth of the film will be defined here in a manner analogous to that used in electrical engineering. The frequency at which the MTF drops to .707 is the upper cutoff frequency. The MTF for most commercial films is available in research literature.[46,47] The fundamental limitation on the MTF frequency response is the grain structure of the film. This must be considered as an additional microscopic diffracting structure which produces unwanted noise. This will be discussed further in Chapter 3.

In what follows, it will also be assumed that the radiation is perfectly monochromatic and spatially coherent.[41] This situation is approximated physically when a laser source is used.

2.2 DESCRIPTION OF A PLANE WAVE

For a given field amplitude component u, the scalar wave equation must be satisfied:

$$\nabla^2 u = \frac{1}{c^2} \frac{\partial^2 u}{\partial t^2} \quad . \qquad (2 - 1)$$

Here, c is the speed of light in the medium through which the wave is propagating, t is time, and ∇^2 is the Laplacian operator in rectangular coordinates defined as

$$\nabla^2 = \frac{\partial}{\partial x^2} + \frac{\partial}{\partial y^2} + \frac{\partial}{\partial z^2} \quad . \qquad (2 - 2)$$

A particular solution of (2 - 1) is

$$u_p(r,t) = A \cos (\omega t - \bar{k} \cdot \bar{r} + \varphi_o) \quad , \qquad (2 - 3)$$

where

$$r = \sqrt{x^2 + y^2 + z^2} \quad , \qquad (2 - 4)$$

and is the magnitude of the position vector $\bar{r}$ defined as

$$\bar{r} = \bar{X}x + \bar{Y}y + \bar{Z}z \quad . \qquad (2 - 5)$$

In this case $\bar{X}$, $\bar{Y}$, and $\bar{Z}$ are unit vectors along the x, y, and z axes respectively. Note that bars will be used to indicate a

vector quantity. The quantity k is the magnitude of the propagation vector $\bar{k}$ defined as

$$\bar{k} = \frac{2\pi}{\lambda}\left[\bar{X}\cos\alpha + \bar{Y}\cos\beta + \bar{Z}\cos\gamma\right]. \qquad (2-6)$$

The cosines of the angles α, β, and γ are the direction cosines of $\bar{k}$ and are determined from the geometry shown in Fig. 3; λ is the wavelength of the propagating wavefront and φ_o is a phase constant. Equation (2 - 3) determines a set of plane waves propagating in the direction $\bar{k}$. This is illustrated in Fig. 3. For a given time t, a surface of constant phase is determined if

$$\bar{k} \cdot \bar{r} = \text{a constant.} \qquad (2-7)$$

This forces the argument of the cosine in Eq. (2 - 3) to remain constant. Condition (2 - 7) determines a plane perpendicular to $\bar{k}$.[48]

If the position vector $\bar{r}$ is in the same direction as $\bar{k}$ then

$$x = r\cos\alpha,$$

$$y = r\cos\beta,$$

$$z = r\cos\gamma, \qquad (2-8)$$

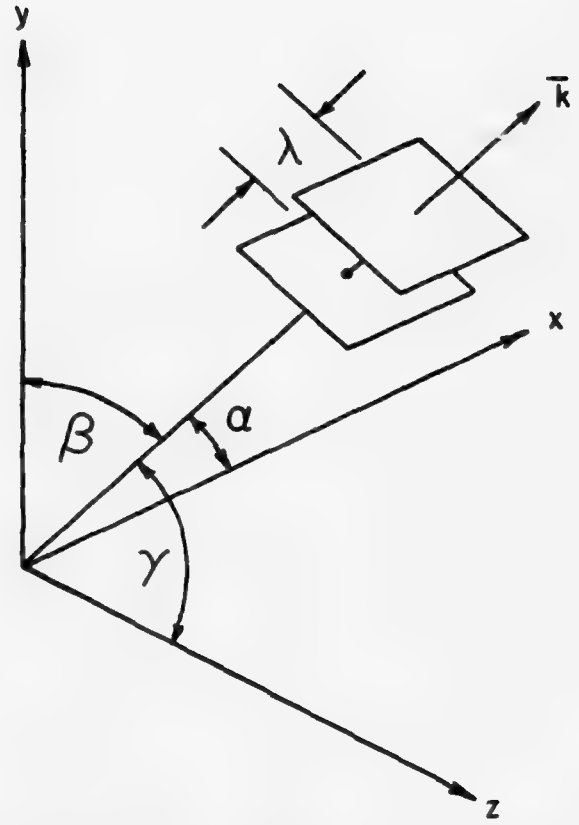

Figure 3. Plane Wavefronts Propagate in the Direction of Vector $\bar{k}$ at a Distance λ Apart.

and from (2 - 5);

$$\bar{r} \cdot \bar{r} = r^2 = x^2 + y^2 + z^2 . \qquad (2 - 9)$$

Substituting the relations given in (2 - 8) into (2 - 9) gives

$$\cos^2 \alpha + \cos^2 \beta + \cos^2 \gamma = 1 . \qquad (2 - 10)$$

Therefore, using (2 - 6) and (2 - 10) gives

$$k = \sqrt{\bar{k} \cdot \bar{k}} = \frac{2\pi}{\lambda} .$$

Also, the scalar product of $\bar{k}$ and $\bar{r}$ in this case is

$$\bar{k} \cdot \bar{r} = \frac{2\pi r}{\lambda} ;$$

this implies that the argument of the cosine in (2 - 3) changes by 2π for a change in r of λ. This means that the distance between planes of equal phase is λ as shown in Fig. 3. As t changes, these surfaces move in the direction of $\bar{k}$ at the phase velocity c.

The direction cosines can be written more concisely if the following definitions are used:

$$L = \cos \alpha,$$

$$M = \cos \beta ,$$

$$N = \cos \gamma .$$

Then, for the position vector $\bar{r}$ in any direction:

$$\bar{k} \cdot \bar{r} = \frac{2\pi}{\lambda} (Lx + My + Nz).$$

With (2 - 10) this equation can be rewritten

$$\bar{k} \cdot \bar{r} = \frac{2\pi}{\lambda} (Lx + My + \sqrt{1 - M^2 - N^2}\, z) ;$$

therefore (2 - 3) becomes

$$u_p (r,t) = A \cos \left[\omega t - \frac{2\pi}{\lambda} (Lx + My + \sqrt{1-M^2-N^2}\, z) + \varphi_o \right] . \qquad (2 - 11)$$

Equation (2 - 11) represents a set of plane waves of frequency ω propagating in a direction determined by two directions cosines: M and N.

2.3 PHASOR REPRESENTATION

The general solution for Eq. (2 - 1) for monochromatic radiation is:

$$u (\bar{r},t) = A (\bar{r}) \cos [\omega t + \varphi (\bar{r})], \qquad (2 - 12)$$

where $A (\bar{r})$ is the amplitude as a function of position and $\varphi (\bar{r})$ is the phase as a function of position. Equation (2 - 12) can be rewritten

$$u (\bar{r},t) = RE [v (\bar{r}) \exp(-j\omega t)], \qquad (2 - 13)$$

and $v (\bar{r})$ is called a "phasor" and is defined as follows:

$$v (\bar{r}) = \exp [-j\varphi (\bar{r})] . \qquad (2 - 14)$$

Re refers to the real part of the quantity in the square brackets of (2 - 13). Actually (2 - 14) by itself is an adequate description of the scalar field $u(\bar{r},t)$. The time dependent part, $\exp(j\omega t)$, is the same for any value of $\bar{r}$ and can always be conveniently added if an explicit representation is desired. The phasor (2 - 14) keeps track of the relative phase of the scalar field at any location. In the rest of this report it will be assumed, unless otherwise stated, that the phasor representation is used to describe any field amplitude.

The equation for a set of plane waves, Eq. (2 - 11), can be conveniently rewritten in phasor form. Let v_p be the associated phasor; then

$$v_p = A \exp\left[j \frac{2\pi}{\lambda} (Lx + My + \sqrt{1-M^2-N^2}\, z) \right]. \qquad (2 - 15)$$

This representation of a plane wave will be very meaningful when the concept of the angular spectrum is considered.

2.4 THE ANGULAR SPECTRUM

When the definition of a two-dimensional Fourier transform given in Chapter 1 is used, the Fourier transform of

the scalar field $t(x_1, y_1)$ is $T(\xi, \eta)$, where

$$T_1(\xi, \eta) = \iint_{-\infty}^{+\infty} t_1(x_1, y_1) \exp[-j 2\pi (x_1 \xi + y_1 \eta)] dx_1 dy_1 . \tag{2 - 16}$$

Using the inverse Fourier transform gives

$$t_1(x_1, y_1) = \iint_{-\infty}^{+\infty} T_1(\xi, \eta) \exp[j 2\pi (x_1 \xi + y_1 \eta)] d\xi \, d\eta . \tag{2 - 17}$$

Equation (2 - 17) has an interesting interpretation if the following equivalences are made:

$$\xi = \frac{L}{\lambda}$$

$$\eta = \frac{M}{\lambda} , \tag{2 - 18}$$

which yields

$$t_1(x, y) = \iint_{-\infty}^{+\infty} T_1\left(\frac{L}{\lambda}, \frac{M}{\lambda}\right) \exp\left[j \frac{2\pi}{\lambda} (L x_1 + M y_1)\right] d\left(\frac{L}{\lambda}\right) d\left(\frac{M}{\lambda}\right). \tag{2 - 19}$$

Note the similarity between the integrand of (2 - 19) and the phasor representation of plane wave given in (2 - 15). The expression

$$T_1\left(\frac{L}{\lambda}, \frac{M}{\lambda}\right) \exp\left[j \frac{2\pi}{\lambda} (L x_1 + M y_1)\right]$$

defines a plane wave of amplitude $T_1(\xi, \eta)$ at $z = 0$ with $\varphi_o = 0$ and direction consines L, M and $\sqrt{1 - L^2 - M^2}$. The

integral of (2 - 19) defines a sum over a continuum of plane waves that are superposed at $z = 0$ to form $t(x_1, y_1)$. The amplitude $T(\xi, \eta)$ represents the amplitude density in plane wave domain description of $t(x_1 y_1)$ and is called the "angular spectrum" at $z = 0$.

2.5 THE PROPAGATED ANGULAR SPECTRUM

The angular spectrum at a distance z from the $z = 0$ plane can now be determined from the phase shift of an arbitrary plane wave. Consider a planewave that travels in the direction of the propagation vector $\bar{k}$. If the wave moves a distance d along the propagation vector, then the phase shift of the displaced wavefront is

$$\exp(jkd)$$

which can be expressed in terms of z. From the geometry,

$$d = z \cos \gamma,$$

but using (2 - 10) gives

$$d = z\sqrt{1 - \cos^2\alpha - \cos^2\beta} = z\sqrt{1 - L^2 - M^2}.$$

Therefore, the additional phase shift of the propagated spectrum is

$$\exp jkz\sqrt{1 - L^2 - M^2},$$

and the propagated angular spectrum T_2 is

$$T_2\left(\frac{L}{\lambda}, \frac{M}{\lambda}, z\right) = T_1\left(\frac{L}{\lambda}, \frac{M}{\lambda}\right) \exp\left(jkz\sqrt{1 - L^2 - M^2}\right). \quad (2 - 20)$$

The propagated spectrum can be used to determine the field amplitude $t_2(x_2, y_2)$ at a distance z from the $z = 0$ plane; this gives

$$t_2(x_2, y_2) = \iint_{-\infty}^{\infty} T_2\left(\frac{L}{\lambda}, \frac{M}{\lambda}, z\right) \exp\left[j2\pi\left(x_2\frac{L}{\lambda} + y_2\frac{M}{\lambda}\right)\right] d\left(\frac{L}{\lambda}\right) d\left(\frac{M}{\lambda}\right),$$

or substituting from (2 - 20)

$$t_2(x_2, y_2) =$$

$$\iint_{-\infty}^{+\infty} T_1\left(\frac{L}{\lambda}, \frac{M}{\lambda}\right) \exp\left[jk\left(x_2L + y_2M + z\sqrt{1 - L^2 - M^2}\right)\right] d\left(\frac{L}{\lambda}\right) d\left(\frac{M}{\lambda}\right). \quad (2 - 21)$$

Therefore, the propagated angular spectrum from a field amplitude distribution $t_1(x_1, y_1)$ can be used to calculate the diffracted field at a parallel plane a distance z away, $t_2(x_2, y_2)$.

2.6 THE FRESNEL APPROXIMATION

The Fresnel approximation to the Huygens-Fresnel Diffraction formula can be derived directly from (2 - 21).

The following approximation can be made by using the binomial theorem:

$$\sqrt{1 - L^2 - M^2} \cong 1 - \frac{L^2}{2} - \frac{M^2}{2} , \qquad (2 - 22)$$

for

$$L << 1 .$$

$$M << 1 .$$

Substituting this approximation into (2 - 21) gives

$$t_2(x_2, y_2) = \exp(j k z) \iint_{-\infty}^{\infty} T_1\left(\frac{L}{\lambda}, \frac{M}{\lambda}\right) \exp\left[-j k z \frac{(L^2 + M^2)}{2}\right]$$
$$\exp\left[j 2\pi \left(x_2 \frac{L}{\lambda} + y_2 \frac{M}{\lambda}\right)\right] d\left(\frac{L}{\lambda}\right) d\left(\frac{M}{\lambda}\right) .$$

Therefore, using the notation for the Fourier transform given in Chapter 1;

$$t_2(x_2, y_2) = e^{j k z} \, F^{-1}\left\{T\left(\frac{L}{\lambda}, \frac{M}{\lambda}\right) \exp\left[-j k z \frac{(L^2 + M^2)}{2}\right]\right\} .$$

Substituting from (2 - 18) gives

$$t_2(x_2, y_2) = \exp(j k z) \, F_1^{-1}\left\{T(\xi, \eta) \exp\left[-j \pi \lambda z (\xi^2 + \eta^2)\right]\right\} . \qquad (2 - 23)$$

Therefore, the field amplitude $t_2(x_2, y_2)$ is found by taking the Fourier transform of the weighted transform of $t_1(x_1, y_1)$. This is more conveniently stated in the space domain using the

convolution theorem discussed in Chapter 1. Since

$$F^{-1}\left\{\exp\left[j\pi\lambda z\,(\xi^2+\eta^2)\right]\right\}=\frac{1}{j\lambda z}\exp\left[jk\,\frac{(x_2^{\,2}+y_2^{\,2})}{2}\right],$$

and

$$F^{-1}\left[T(\xi,\eta)\right] = t_1\,(x_1,y_1)\;;$$

the convolution theorem gives

$$t_2\,(x_2,y_2) =$$

$$\frac{\exp\,(jkz)}{j\lambda z}\iint_{-\infty}^{\infty} t_1\,(x_1,y_1)\,\exp\left\{\frac{k}{2z}\left[(x_2-x_1)^2-(y_2-y_1)^2\right]\right\}dx_1dy_1. \qquad (2-24)$$

Equation (2 - 24) is known as the Fresnel approximation. It represents a very useful approximation to the Huygens-Fresnel diffraction integral in terms of a linear spatially invariant mapping. Certain assumptions are tacitly implied in its use. The approximation given in (2 - 23) implies that cos γ be very small, or that the angle of diffraction is small. The quadratic term in the exponential of the integral represents a quadratic approximation to a spherical wave.[42] This is valid if

$$z >> \sqrt{(x_2-x_1)^2+(y_2-y_1)^2}\quad . \qquad (2-25)$$

Also, it should be pointed out that the integral from $-\infty$ to $+\infty$ in Eq. (2 - 23) requires $\left|\frac{L}{\lambda}\right|$ and $\left|\frac{M}{\lambda}\right|$ to exceed 1 , which implies that the value of the direction cosines exceeds 1. This is possible for complex arguments and physically represents evanescent waves. These waves propagate in the x and y directions, but die off exponentially in the z direction. Since they die off so rapidly, their effect can be neglected.[42]

2.7 THE PHASE SHIFT MODEL OF A THIN LENS

The classical "thin" spherical lens can be effectively modeled using a quadratic phase shift.[42] If the lens is assumed infinite in size with a focal length f, then it can be described by the following complex transmittance:

$$\exp\left[j\frac{k}{2f}\,(x^2 + y^2)\right] . \qquad (2 - 26)$$

It is assumed that the lens is infinitesimally thin and fills the x - y plane. A real lens with a finite thickness is fairly well modeled using (2 - 26). The effect of most thick lenses is to translate the diffracted field slightly along the optical axis by the distance between its principal planes. Usually

this distance is small enough to be neglected. Where a multielement lens is used, the focal length of the effective thin lens is measured from the principal planes of the multielement system. This is usually a minor problem in using a lens for an optical computer, since it primarily effects certain scaling factors that are easy to measure directly and can be accounted for without a more exact model of the lens using its principal planes.

The ideal lens described above can be used to perform very complex optical computations using the field amplitudes. The most important of these is the two-dimensional Fourier transform.

2.8 OPTICAL COMPUTATION OF THE FOURIER TRANSFORM

The lens arrangement shown in Fig. 4 can be used to calculate the two-dimensional Fourier transform of an arbitrary field amplitude distribution $b(x_1, y_1)$. The Fourier transform $B\left(\frac{x_3}{\lambda f}, \frac{y_3}{\lambda f}\right)$ occurs in the back focal plane of lens L_1. This can be shown by straightforward application of the Fresnel approximation to the optical system.

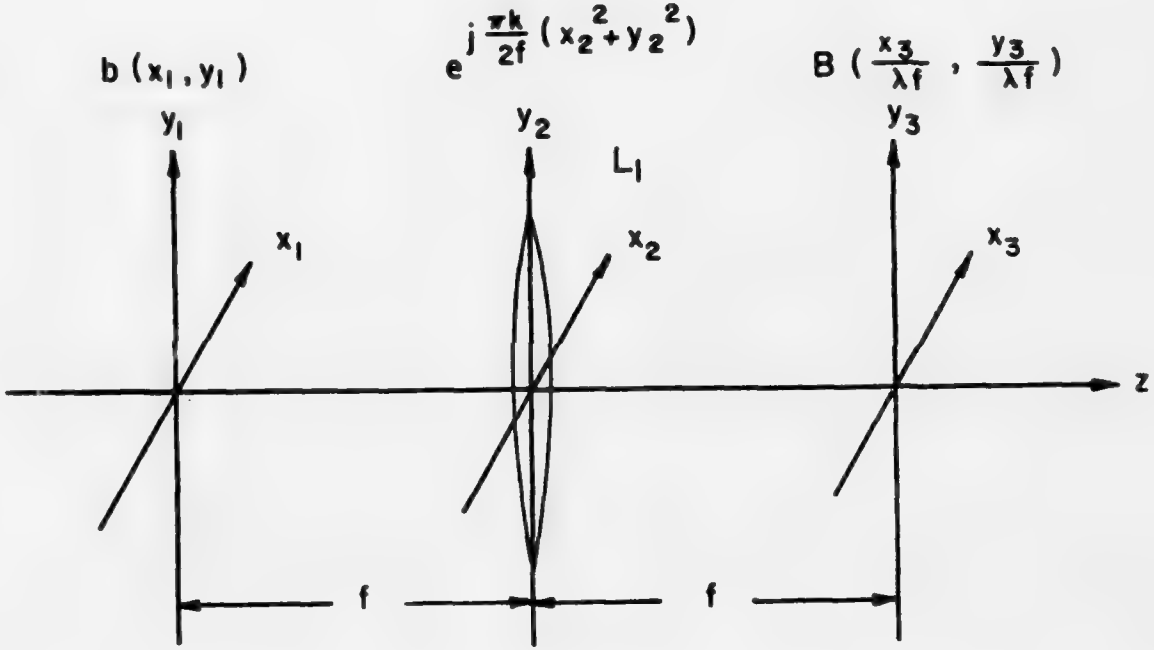

Figure 4. Lens Arrangement Used to Compute the Fourier Transform of $b(x_1, y_1)$. The Fourier Transform Occurs in the x_3-y_3 Plane.

The diffracted field from $b(x_1, y_1)$ at the front side of lens L_1 is $p(x_2, y_2)$. This is calculated directly from Eq. (2 - 24). This gives

$$p(x_2, y_2) =$$

$$\frac{\exp(jkf)}{j\lambda f} \iint_{-\infty}^{\infty} b(x_1, y_1) \exp\left\{\frac{k}{2f}\left[(x_2 - x_1)^2 + (y_2 - y_1)^2\right]\right\} dx_1 dy_1 \ .$$

The field at the back side of lens L_1 is $p'(x_2, y_2)$ where

$$p'(x_2, y_2) = p(x_2, y_2) \exp\left[\frac{k}{2f}(x_2^2 + y_2^2)\right] \ .$$

The field a distance f in back of L_1 is then $q(x_3, y_3)$, where

$$q(x_3, y_3) =$$

$$\frac{\exp(jkf)}{j\lambda f} \iint_{-\infty}^{+\infty} p'(x_2, y_2) \exp\left\{\frac{jk}{2f}\left[(x_2 - x_1)^2 + (y_2 - y_1)^2\right]\right\} dx_2 dy_2 \ .$$

If q is expressed in terms of b directly, this yields

$$q(x_3, y_3) = -\frac{\exp(2jk)}{\lambda^2 f^2} \iiint_{-\infty}^{+\infty} b(x_1, y_1) \exp\left[\frac{jk}{2f}(x_1^2 + y_1^2)\right]$$

$$\exp\left[\frac{jk}{2f}(x_2^2 + y_2^2)\right] \exp\left[\frac{jk}{2f}(x_3^2 + y_3^2)\right]$$

$$\exp\left\{-\frac{jk}{f}\left[x_2(x_3 + x_1) + y_2(y_3 + y_1)\right]\right\} dx_1 dy_1 \, dx_2 dy_2 \ . \qquad (2 - 27)$$

This cumbersome integral can be reduced by carrying out part of the integration with respect to x_2 and y_2. Note that this integration can be viewed as the Fourier transform of a two-dimensional Guassian[42]

$$\int_{-\infty}^{+\infty}\int \exp\left[\frac{j\pi}{\lambda f}(x_2^2 + y_2^2)\right]$$
$$\exp\left\{-j2\pi\left\{x_2\left[\frac{(x_3+x_1)}{\lambda f}\right] + y_2\left[\frac{(y_3+y_1)}{\lambda f}\right]\right\}\right\} dx_2\, dy_2 =$$
$$j\lambda f \exp\left[-j\frac{k}{2f}(x_3^2 + y_3^2)\right] \exp\left[-j\frac{k}{2f}(x_1^2 + y_1^2)\right]$$
$$\exp\left[-j\frac{k}{f}(x_3x_1 + y_3y_1)\right] .$$

Thus the integral in (2 - 28) simplifies to

$$p(x_3, y_3) =$$
$$\frac{\exp(2jk)}{j\lambda f}\int_{-\infty}^{+\infty}\int b(x_1, y_1) \exp\left[-j2\pi\left(x_1\frac{x_3}{\lambda f} + y_1\frac{y_3}{\lambda f}\right)\right] dx_1\, dy_1 . \qquad (2 - 28)$$

This integral is the Fourier transform of $b(x_1, y_1)$. The frequency domain variables in this case are $\frac{x_3}{\lambda f}$ and $\frac{y_3}{\lambda f}$. Therefore, except for a multiplicative constant an exact Fourier transform of $b_1(x_3, y_3)$ occurs in the back focal plane of L_1. The lens L_1 can be thought of as an optical

computer. With two lenses it is possible to carry out filtering operations in the back focal plane of a lens and recover the filtered image with an additional lens. This will be explained in the next chapter.

CHAPTER 3

MULTICHANNEL IMAGE DECODING

In Chapter 1, a decoding scheme using an inverse filter was discussed. It was pointed out that in practice it is not possible to recover information in the frequency plane where the coding transfer function has zeros or approaches zero, due to limitations set by noise. In this chapter a very general scheme is introduced that can improve the signal-to-noise ratio and increase the amount of information recovered in a decoding operation. It will be shown that coding an image with more than one code can be advantageous. Each version of the coded image is a separate information "channel" which can be used to recover the decoded image. An application of this multiple-coding scheme will be examined in detail for the case of severe misfocus blurring.

3.1 FINITE RANGE INVERSE FILTERS

Since the dynamic range of inverse filters is noise-limited, inverse filters with a finite dynamic range will be considered. In regions where the signal-to-noise ratio prevents recovery of a particular point in the frequency plane, the value of the inverse decoding filter becomes arbitrary. For example, the filter has simply been set to the maximum value.[24] However, when noise is studied in more detail, it is better handled using a linear optimal estimator. A linear least-mean-square error inverse filter T for the coding transfer function H is[49]

$$T = H^{-1}\left[\frac{\sigma}{\sigma + |H|^{-2}}\right] . \qquad (3-1)$$

Here σ is the signal-to-noise ratio defined in the frequency domain as the ratio of the Wiener spectrum of the coded image to the Wiener spectrum of the noise. In common practice the recording is usually made on photographic film and the noise is primarily grain noise. σ is usually approximated by a constant. For fine grain emulsions, σ ranges from 10^2 to 10^4. The filter T minimizes the mean square error in the intensity difference between the original image before coding and the

decoded image using a linear estimate. This means that the decoded image is described as weighted sum (or a weighted integral in the continuous case) of the coded image intensity values.

In the work which follows, a simplification of the filter T will be used. A reasonable approximation to T is the finite inverse filter H_F^{-1} where [30]

$$H_F^{-1} = H^{-1} \quad \text{if} \quad 1 \geq |H| \geq D^{-1}$$

and

$$H_F^{-1} = 0 \qquad \textit{elsewhere.} \qquad (3-2)$$

D is the dynamic range. It is assumed for convenience that H is normalized such that its maximum value is 1. When this filter is used to carry out a decoding operation, the relationship between the uncoded image S and the decoded image S' can be described by an effective transfer function H_R. Following Tichenor, this transfer function will be referred to as the "restored" transfer function. Therefore, in equation form

$$H_R = H_F^{-1} H \qquad (3-3)$$

and

$$S' = H_R S \ . \qquad (3 - 4)$$

Note that $H H_F^{-1}$ must be 1 or 0; therefore H_R is a binary function such that

$$H_R = 1 \qquad |H| \geq D$$

$$H_R = 0 \qquad \text{elsewhere} \ . \qquad (3 - 5)$$

3.2 MULTICHANNEL IMAGE DECODING WITH A COMPOSITE FILTER

Consider an object coded using n different codes to create n separate coded images or channels. For the ith channel, the output g_i is the convolution of the image with an impulse response h_i. Therefore,

$$g_i = h_i * s. \qquad (3 - 6)$$

The impulse response for each channel is different. In the frequency domain, the output for the ith channel is

$$G_i = H_i S. \qquad (3 - 7)$$

The upper-case variables in the frequency domain correspond to lower-case variables in the space domain. A particular point $S(\xi, \eta)$ in the frequency domain can be recovered using the inverse filter for any channel. Multiplying through (3 - 7)

by the inverse for the ith channel gives

$$H_i^{-1}(\xi,\eta)\, G_i(\xi,\eta) = H_i^{-1}(\xi,\eta)\, H_i(\xi,\eta)\, S(\xi,\eta)$$

or

$$S(\xi,\eta) = H_i^{-1}(\xi,\eta)\, G_i(\xi,\eta) \qquad (3-8)$$

In general any channel can be used to attempt a recovery of $S(\xi,\eta)$. There is complete freedom to choose the channel that maximizes the signal-to-noise ratio. The total effect of selectively choosing between different channels for recovering frequency domain information is a "composite" coding transfer function and a composite decoding inverse filter. The image can be thought of as coded with a single transfer function that is made up from a mosaic using pieces of the original n coding transfer functions. Associated with this composite coding function is a composite decoding filter. For a normalized composite coding transfer function H_C, the inverse filter or decoding filter is H_C^{-1}. The information recovered using H_C^{-1} can be maximized by carefully choosing the combination of codes used. This will be demonstrated later using a two-channel code.

In practice, an image coded with a transfer function

H_c must be decoded with a finite range inverse filter H_{CF}^{-1}. If the approximation to the mean square error filter described in (3 - 2) is used, then H_{CF}^{-1} is defined as

$$H_{CF}^{-1} = H_C^{-1} \quad \text{if} \quad 1 \geq |H_C| \geq D$$

$$H_{CF}^{-1} = 0 \qquad \text{elsewhere.} \qquad (3 - 9)$$

The resulting restored transfer function H_{CR} is, using (3 - 5),

$$H_{CR} = 1 \qquad \text{if} \qquad |H_C| \geq D$$

$$H_{CR} = 0 \qquad \text{elsewhere.} \qquad (3 - 10)$$

If the composite transfer function is to maximize the signal-to-noise ratio, then

$$|H_C| \geq D^{-1} \qquad \text{iff.} \quad |H_i| \geq D^{-1} \text{ for at least one } i.$$

Therefore

$$H_{CR} = 1 \qquad \text{iff.} \quad |H_i| \geq D^{-1} \text{ for at least one } i.$$

$$H_{CR} = 0 \qquad \text{elsewhere.} \qquad (3 - 11)$$

For a given point, $S(\xi, \eta)$ can be recovered and $H_{CR} = 1$ if any one of the coding channels has a coding function $|H_i(\xi, \eta)| \geq D^{-1}$. Using (3 - 5), if the decoded image is S', gives

$$S' = H_{CR} S \ . \qquad (3 - 12)$$

Equation (3 - 12) will be useful in the optical simulation to be described.

3.3 SEVERE MISFOCUS BLURRING

As an example of a multichannel decoding application, misfocus blurring will be used. When an aberration free lens, stopped with a round aperture, is used to form a severely misfocused image, the normalized transfer function associated with the blur-coded image is approximately [51]

$$H_A(\rho) = \frac{2 J_1(\pi\rho)}{\pi\rho} , \qquad (3 - 13)$$

where $\rho = \xi^2+\eta^2$ is the frequency domain variable; H_A is circular symmetric. The equation (3 - 13) is accurate for extreme misfocus where diffraction effects can be ignored. In the space domain, this represents a convolution of the original object with a circular disk. This also corresponds to coded aperture imaging where the coding aperture is circular. A plot of this function is shown in Fig. 5 for a dynamic range of 100. The phase and log of the magnitude are plotted separately. Figure 6 shows the finite range inverse filter used to decode an image coded using (3 - 13).

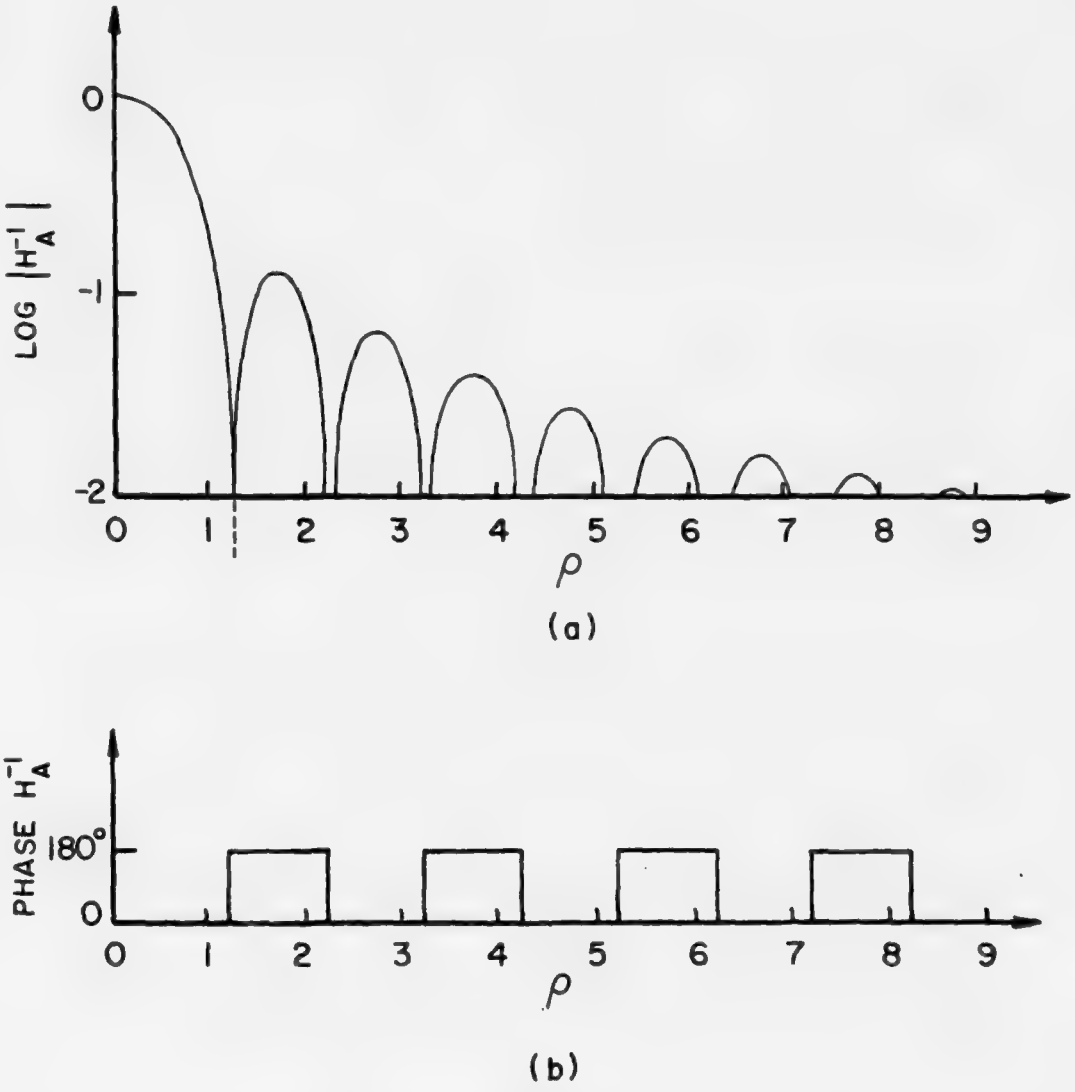

Figure 5. Transfer Function for Severe Misfocus Blur. (a) Log of the Magnitude of H_A; (b) Phase of H_A.

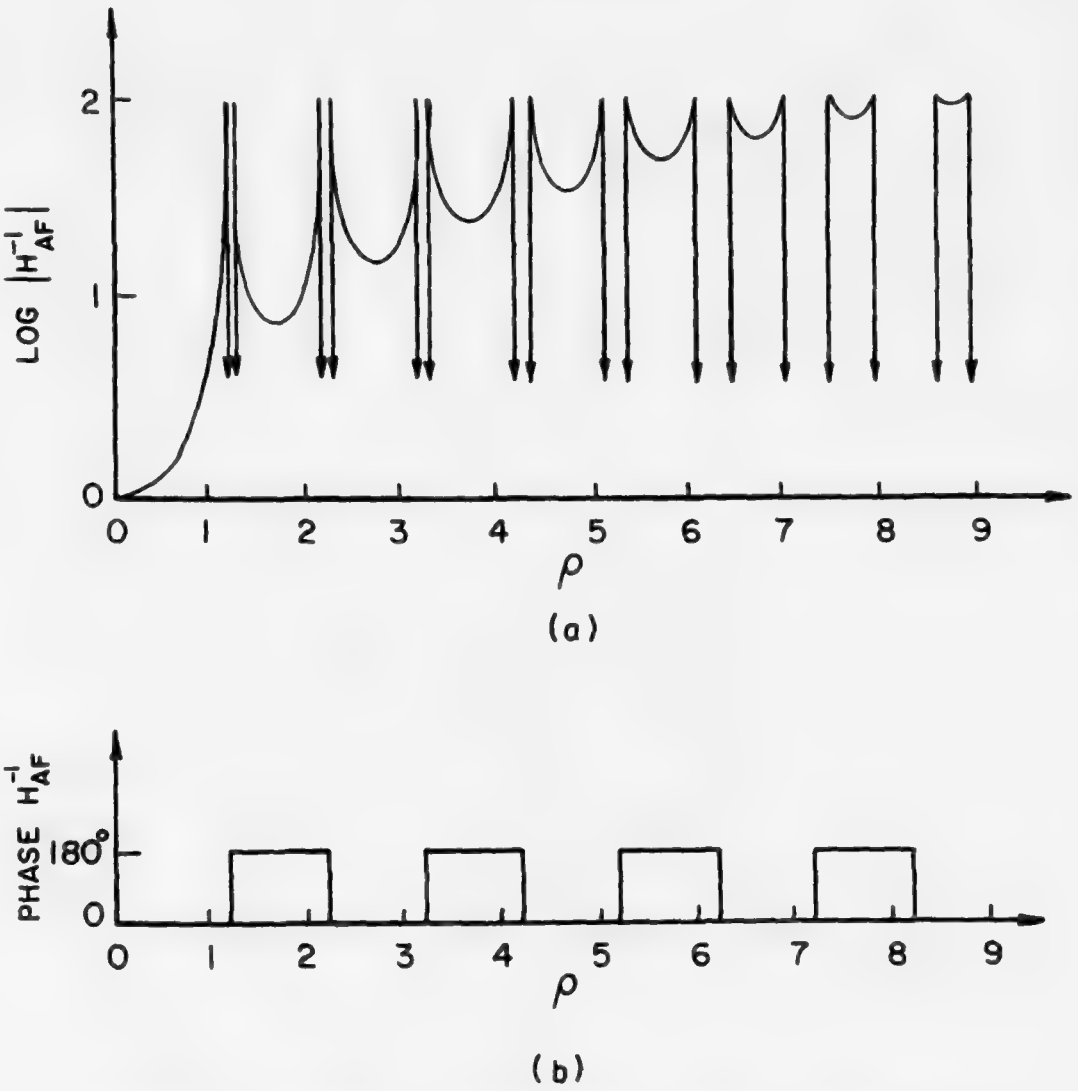

Figure 6. Finite Range Inverse Filter for Severe Misfocus Blur. (a) Log of the Magnitude of H_{AF}^{-1}; (b) Phase of H_{AF}^{-1}. The Arrows in Fig. (a) Approach Minus Infinity.

3.4 A TWO-CHANNEL DECODING SCHEME

A multichannel coding scheme can be formulated using the blur code just discussed. Let an image be coded using the following two codes:

$$H_A(\rho) = \frac{2 J_1(\pi \rho)}{\pi \rho} \qquad (3 - 14)$$

$$H_B(\rho) = \frac{2 J_1(\pi \Delta \rho)}{\pi \Delta \rho} \qquad (3 - 15)$$

where Δ is a constant such that $\Delta \geq 1$. Physically, this corresponds to blurring the image twice with different amounts of blurring. If the image is decoded with a two-channel finite range inverse filter with a dynamic range D, then using (3 - 11) the restored transfer function H_{R2} is

$$H_{R2} = 1 \quad \text{where} \quad |H_A| \geq D^{-1} \text{ or } |H_B| \geq D^{-1}$$

$$H_{R2} = 0 \qquad \text{elsewhere.} \qquad (3 - 16)$$

For comparison, the one-channel code using (3 - 14) has a restored transfer function H_{R1}, where

$$H_{R1} = 1 \quad \text{where} \quad |H_A| \geq D^{-1};$$

$$H_{R1} = 0 \qquad \text{elsewhere.} \qquad (3 - 17)$$

H_{R1} has only one condition for recovery of information, while H_{R2} has two. By carefully choosing Δ, it is possible to optimize, in some sense, the information recovered.

3.5 A GRAPHICAL ANALYSIS

The constant Δ is a scaling factor that is used to "contract" the transfer function H_B. If Δ is properly chosen, the transfer function H_B will overlap in the zero regions of H_A in the composite transfer function. This can be used to eliminate zero regions in the restored transfer function. Ideally, Δ should be adjusted for the particular image being coded. Different values of Δ should be tried until the "best" image is decoded in some sense, such as determined by a mean square error criterion or judgment by eye. However, adjusting Δ for each image would be a difficult task. Instead, it might be more useful to find a criterion for a nonspecific image. A particularly easy criterion to carry out analytically is to maximize the frequency range up to the first zero in the restored transfer function. The justification for this criterion will be given later using an optical simulation, where the eye can judge and compare two-channel versus one-channel coding and decoding.

To optimize Δ, a digital computer can be used. For a given dynamic range D, the restored transfer functions are determined from (3 - 16) for different values of Δ. The Δ which maximizes the frequency range to the first zero determines the optimal code. This was tried but was found to require an excessive amount of computer time. A better plan involving a graphical approach was used.

If the two coding transfer functions were plotted together on the same graph, the frequency range from ρ=0 to the first zero in H_{R2} can be read directly. For a given dynamic range, it is necessary only to observe the frequency range up to which the absolute magnitude of at least one of the transfer functions stays above the dynamic range. This procedure would require a different set of graphs for each Δ. This can be avoided by plotting the transfer functions versus log ρ instead of ρ. Since

$$\log (\Delta \rho) = \log \Delta + \log \rho , \qquad (3 - 18)$$

a change in Δ or the scaling of H_B requires only a shift in position. It is necessary only to plot two identical transfer functions (in this case $2 J_1(\pi \rho)/\pi \rho$) and move one transfer

function relative to the other along the log ρ axis a distance log Δ. To facilitate the shifting of the transfer functions, two identical plots of H_A were made on separate pieces of trace paper. The plotted graphs were then superposed on a light table and could be moved relative to one another. The plots were made using a digital computer and a Calcomp plotter. The log of the transfer function modulus was plotted instead of the modulus to ease reading small values and allow dynamic ranges from 0 up to 100 to be read from one graph. The Calcomp plot is shown in Fig. 7. The graph is on a 10" by 20" rectangular grid and is accurate to .02". By trial and error, it was easy to shift the relative positions of the graphs to maximize the frequency range to the first zero in the composite restoring function H_{R2}.

The results of this analysis are shown in Fig. 8. The solid line shows the maximized frequency range up to the first zero of H_{R2}. This can be compared with range to the first zero of H_{R1}, shown by the dotted line. Above $D \simeq 8$, the two-channel scheme becomes advantageous. H_{R1} has information "gaps" located near the zeros of H_A. Therefore information is missing in regions near $\rho \simeq 1.2, 2.2, 3.2$, etc.; these are the

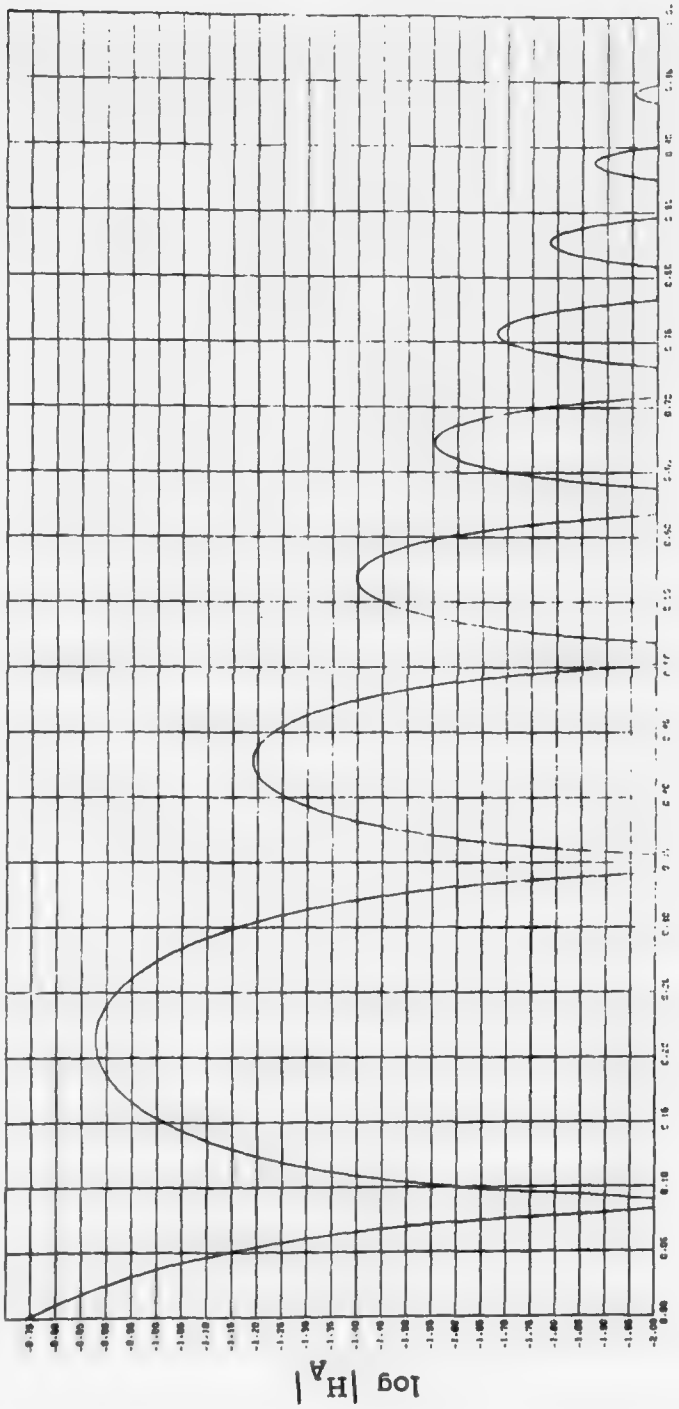

Figure 7. Plot of the Log of the Magnitude of the Blur Coding Transfer Function, H_A', Versus Log ρ Made on a Calcomp Plotter.

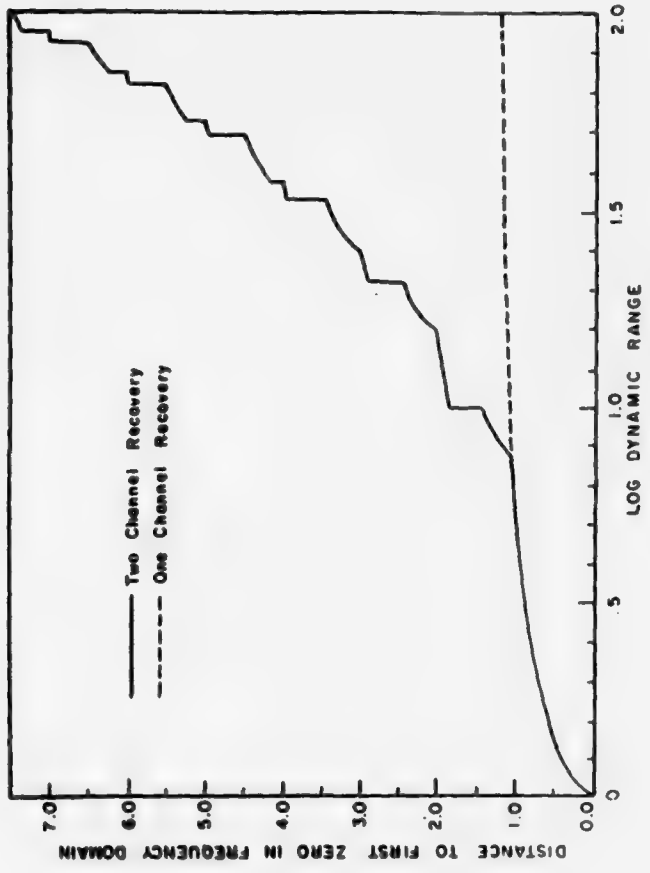

Figure 8. Frequency Range up to the First Zero in the Restored Transfer Function for One-Channel and Two-Channel Decoding Versus Log D.

roots of H_A. When the first zero of H_{R2} lies beyond one of these regions, the two-channel filter can fill in or "bridge" the information gap. The location of the first zero can shift abruptly. These shifts are located at points where a gap has just been bridged in one channel by the other. The slope discontinuities are due to the different rates at which the zero shifts with dynamic range in the two different channels. The distance to the first zero for H_{R2} varies approximately as $D^{.7}$.

3.6 BINARY DENSITY PLOTS OF THE RESTORED TRANSFER FUNCTIONS

It is interesting to make binary density plots of H_{R1} and H_{R2} in the frequency plane for a specific dynamic range. A range with D=100 represents about the best "state of the art" inverse filter used in optical filtering. This compares well with the range of digital computers which are limited by input scanners. Typical scanners have a dynamic range of about 128.[52]

Figure 9 shows the binary density plots of H_{R1} and H_{R2} for D=100. The regions in the frequency domain where the restored transfer functions equal one are shown in white.

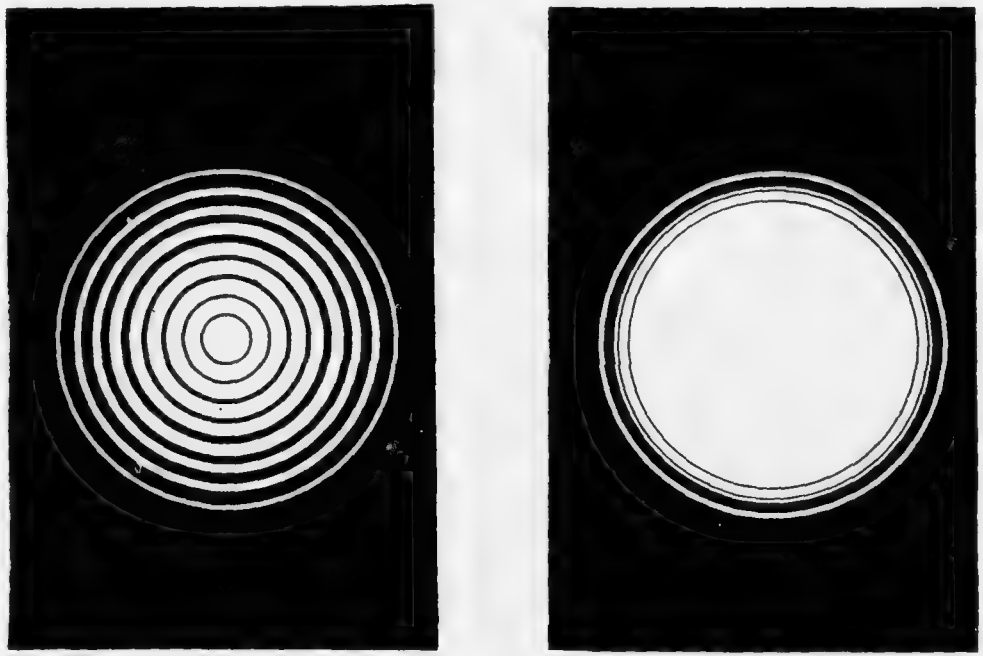

(a) (b)

Figure 9. Binary Density Plots of Restored Transfer Functions H_{R1} and H_{R2}. H_{R1} is Shown in (a); H_{R2} is Shown in (b).

The black indicates areas where the restored transfer functions are zero. In Fig. 9(a), the black annuluses indicate information gaps near the zeros of H_A. In Fig. 9(b), H_{R2} shows recovery of information near the first six zeros of H_{R1}. Two-channel decoding yields about 37% more recovered area in the frequency domain. The maximum spatial frequency at which information is retrieved in Fig. 2(b) occurs at $\rho \simeq 8.9$.

3.7 VALIDITY OF THE CRITERION USED

The criterion discussed for maximizing Δ has shown to be of great value in eliminating frequency domain information gaps nears zeros. It should be pointed out that the accuracy of the finite range inverse filter used to model decoding assumes that the coded images have a low noise content.[30] This assumes that D^{-1} is much greater than the signal-to-noise ratio. This is the case in the examples discussed in Section 3.6 where the dynamic range can be one or two orders of magnitude above film grain noise. This assumption is necessary in the optical simulation to be discussed where noise is neglected. In this case, an optical simulation using only the restored transfer functions gives a valid comparison between one- and

two-channel decoding.

3.8 AN OPTICAL SIMULATION OF TWO-CHANNEL AND ONE-CHANNEL DECODING

The restored transfer functions for the case of one-channel and two-channel coding can be used to compare the two decoding schemes. Since the decoded image is related to the coded image directly using the restored transfer function, (see Eq. (3 - 12)) a comparison was made between the two different codings using only the restored transfer functions. Equation (3 - 12) was implemented using an optical computing arrangement.

In Chapter 2 it was shown that a lens can be used to compute the Fourier transform of a given E-field distribution. If a transparency with an E-field transmittance proportional to some arbitrary test image $s(x,y)$ is placed in a collimated laser beam, then an E-field distribution proportional to the image distribution is obtained. This situation is shown in Fig. 10. A lens L_1 with a focal length f_1 is used to get a scaled Fourier transform in the back focal plane of the lens. (See Eq. (2 - 12).)

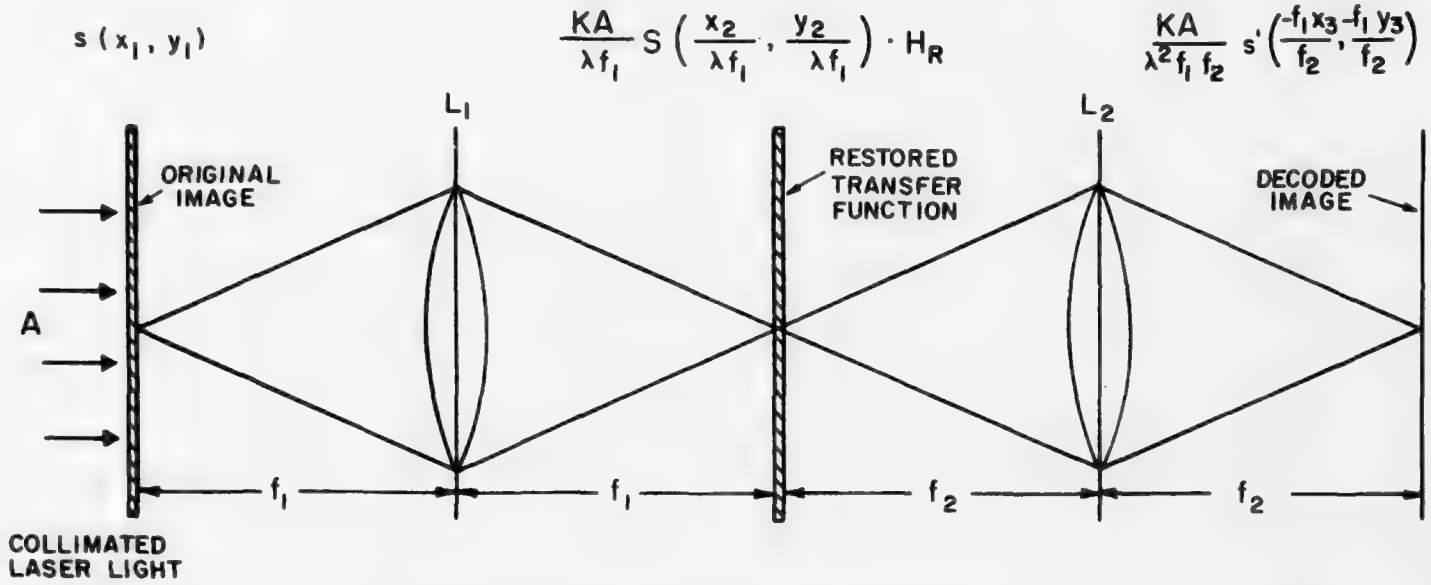

Figure 10. Using the Lens Arrangement Shown Above, the Effects of Coding and Decoding s to get a Decoded Image s′ can be Simulated Using a Transparency of the Restored Transfer Function in the Frequency Plane.

The effect of a coding-decoding operation requires multiplication of the Fourier transform by the restored transfer function H_R to get the decoded image transform $S'(x,y)$. This is accomplished by placing a transparency proportional to H_R, that is KH_R, in the frequency plane; K is a constant. The product,

$$\frac{KA}{\lambda f_1} S\left(\frac{x_2}{\lambda f_1}, \frac{y_2}{\lambda f_1}\right) H_R ,$$

occurs in the frequency plane. Lens L_2 performs another scaled Fourier transform to recover the decoded image. The image is inverted, since two forward transforms have occurred; [42] this gives

$$\frac{KA}{\lambda^2 f_1 f_2} S'\left(\frac{-f_1 x_3}{f_2}, \frac{-f_1 y_3}{f_2}\right) .$$

Using the lens system described above with the restored transfer functions for one- and two-channel decoding, a simulation was carried out to compare the two different codings on several images.

3.9 THE EXPERIMENTAL SETUP

The optical bench setup used in carrying out the simulation is shown in Fig. 11. The lens system of Fig. 10 is used. The lens L_1 is 75 mm in diameter with $f_1 = 300$ mm. L_2 is 50 mm in diameter with a focal length of 330 mm. Using geometrical optics, the largest ray angle of a point on axis in the input plane that reaches the output plane is $\simeq 4,8°$. This gives a frequency cutoff near 130 lines/mm for a wavelength of 6238A. The transparencies used were rectangular with an aspect ratio that varied for different subjects. The cutoff frequency for the recorded image on the transparencies was about 30 lines/mm, well below the optical system bandwidth. Since the transparencies were small, the off-axis points had approximately the same bandwidth; thus the effects of the lens stops were negligible.

A television vidicon was placed in the output plane of the optical system. The decoded image was observed on a 9-inch diagonal monitor. A Polaroid camera with a closeup kit was used to record from the monitor. Using the television camera had several advantages: it gave a large bright image

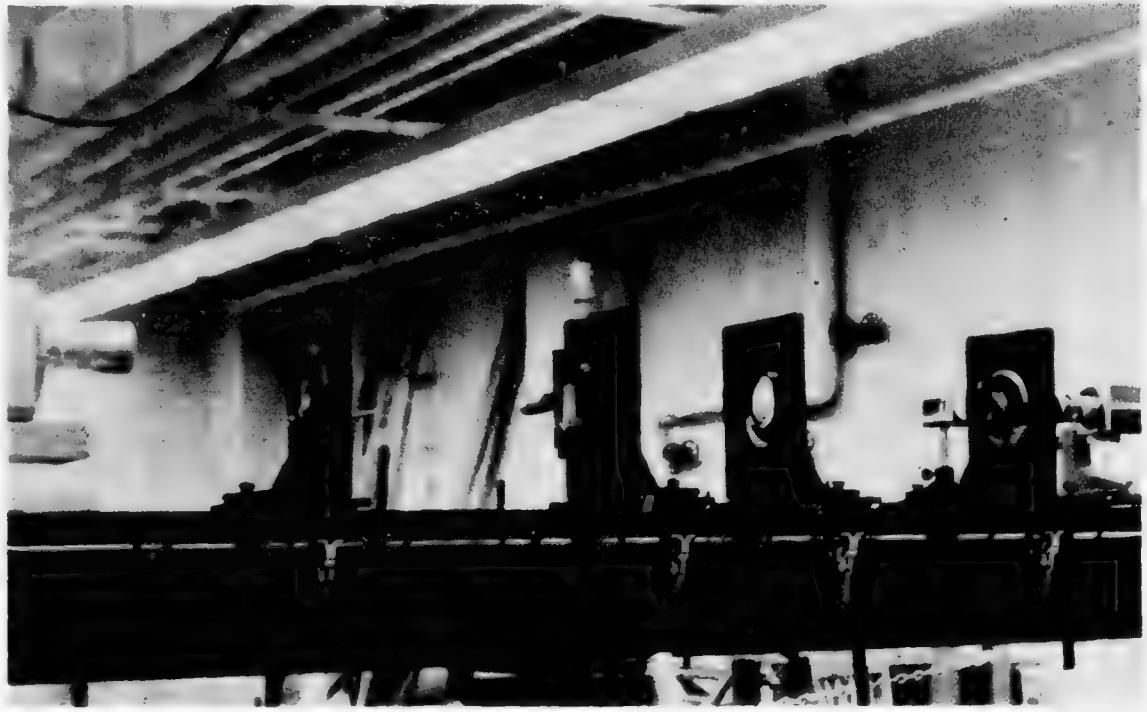

Figure 11. Optical Bench Arrangement for Simulation. From Left to Right: Television Vidicon, Lens L_2, Liquid Gate for Filter in x-y Translator, Lens L_1, Liquid Gate for Subject Transparencies, and Collimating Lens and Laser with a Spatial Filter.

that was easy to view and photograph, it allowed the contrast to be adjusted for best viewing, and it eliminated speckling effects. The speckling was eliminated due to its low pass frequency characteristics. In terms of the size of the images viewed, the cutoff was about 35 lines/mm.

The restored transfer functions were photographed from the drawings shown in Fig. 9. The filters were reduced to a diameter of 1.5 mm. (The diameter is measured out to the highest frequency passed.) This required a reduction of about 92X from the original drawings. This was accomplished by photographing in two stages. The filters were first reduced 10X by photographing them on Kodak high contrast copy film. A contact print positive was then made on Kodalith film. This positive was then used to make a negative print on Kodak polycontrast F resin-coated paper. A second reduction of about 9X was made by photographing the negative print with a 35 mm camera on Kodak high contrast copy film. This produced a reduced positive of the original transfer functions. Since the restored transfer functions were binary functions, the E field transmittance was the same as the intensity transmittance.

It was only necessary to get as much contrast as possible in the recorded images. The high contrast film used had a $\gamma \simeq 5$. Under a microscope, the recorded filters showed good contrast and only a small amount of edge spreading.

The subjects used in testing were reductions made from mounted photographs. The transparency negatives were made on Kodak panatomic film and developed to a $\gamma = .6$. The negatives were then contact printed on Kodak fine grain positive release film, which was developed to a $\gamma \simeq 1.6$. This gave a low contrast positive with a $\gamma \simeq 1$. The test subjects were in a rectangular format against a dark background. It can be shown that a low contrast intensity recording produces an E-field transmittance proportional to the intensity of the recording. This was originally discussed by Tsuchichu and his results are given in Appendix I.

The test transparencies and the restored transfer functions were mounted in liquid gates to reduce phase distortions caused by thickness variations in the photographic emulsion. The liquid gate consists of two optically flat pieces of glass between which the photographic transparency

is placed in an index-matching fluid. The index-matching fluid is chosen to match the index of refraction of the photographic gelatin, about 1.51. The gate for the restored transfer function was mounted on an x-y translator. This allowed accurate positioning of the filters in the Fourier transforms plane.

A spoke pattern was used to position the filters accurately. When the restored transfer functions were properly aligned, the spoke showed a circularly symmetric pattern of straight spokes with notches at the missing frequencies. When the filters were misaligned or phase distortions were present, the spoke pattern was not symmetric and showed "kinks" in the spokes. Once the spoke pattern was aligned, it was replaced with a test transparency, and the simulated decoded image was photographed.

3.10 TEST RESULTS

Results of the optically computed simulation are given in Figs. 12 through 17. The subjects are designated by numbers 1, 2, 3. Each subject has four pictures associated with it:

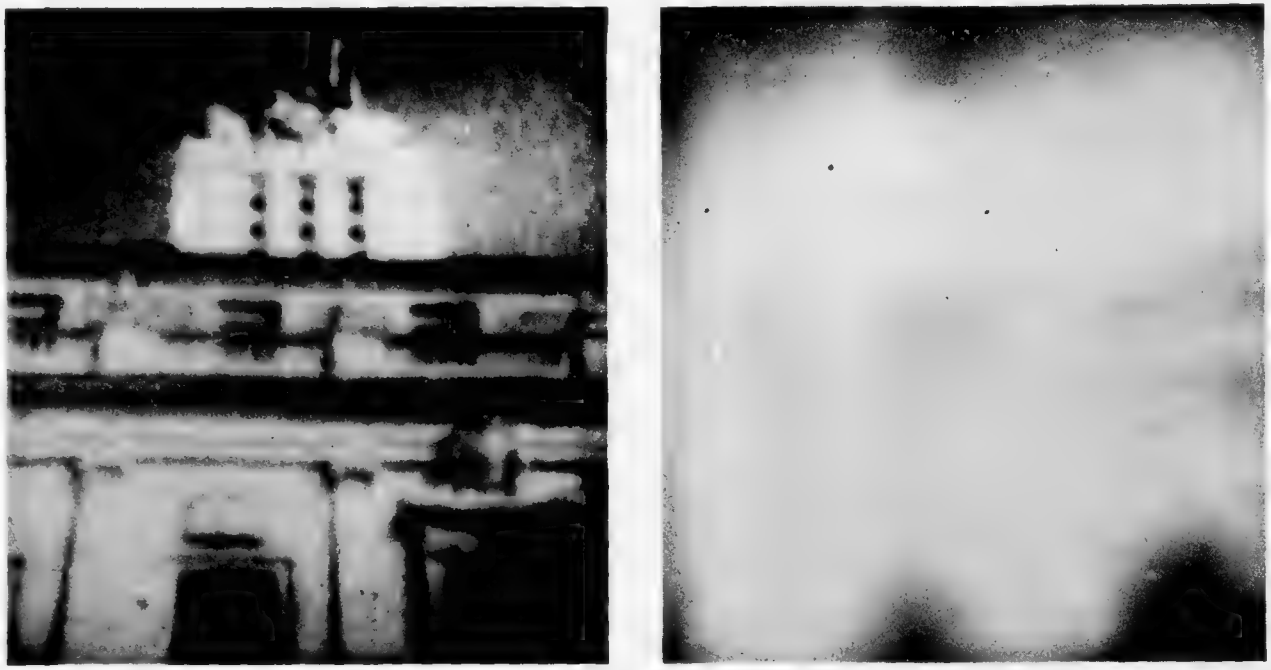

(a) (b)

Figure 12. Test Subject No. 1. (a) Unfiltered Subject as Viewed on the Vidicon Monitor; (b) Blur Coded Image.

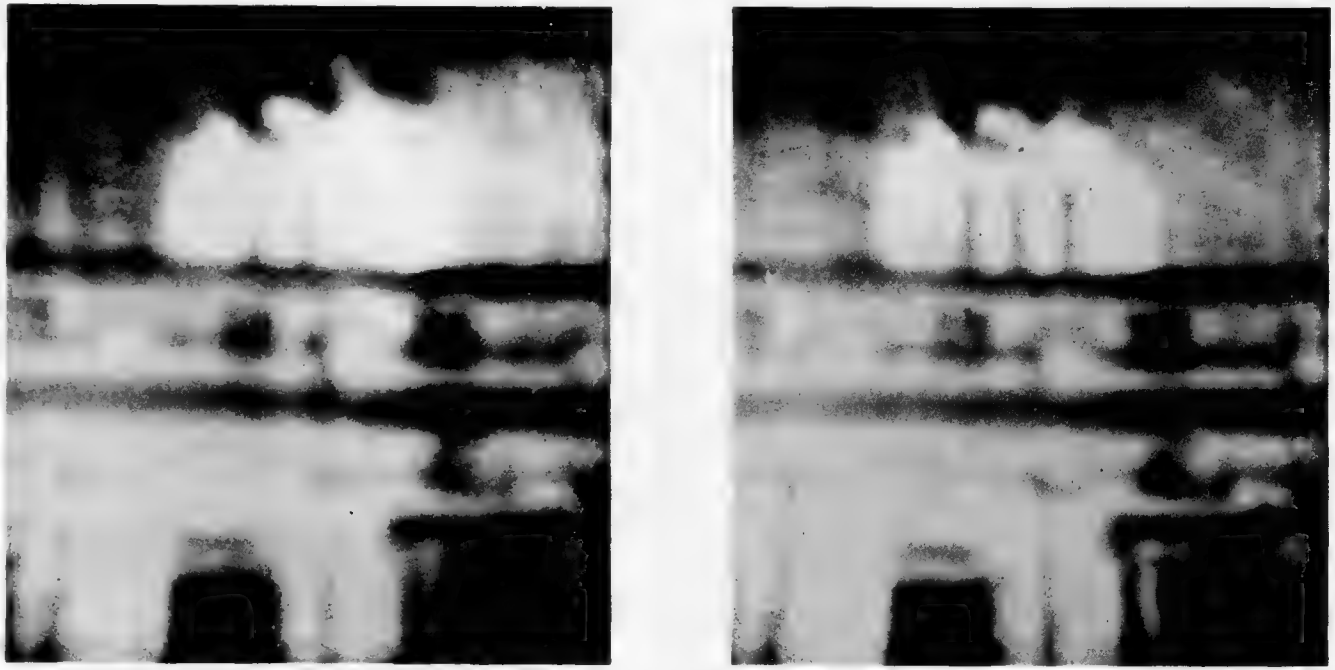

(a) (b)

Figure 13. Test Subject No. 1. (a) Simulated Decoded Image Using One-Channel Decoding; (b) Simulated Decoded Image Using Two-Channel Decoding.

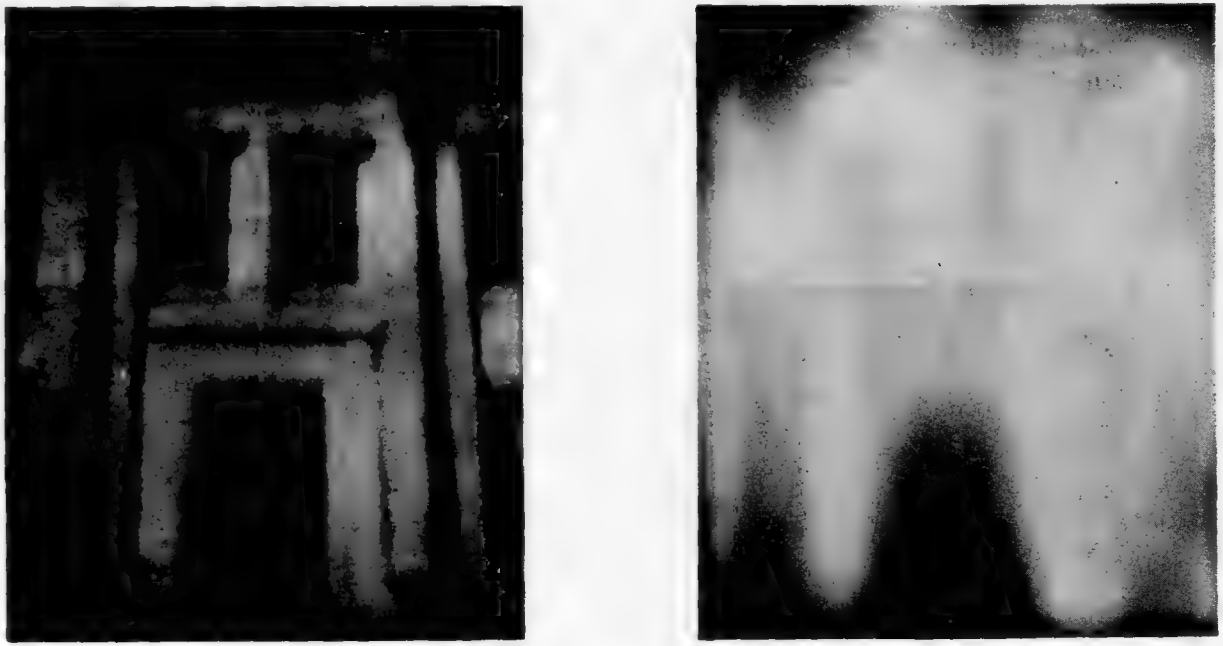

(a) (b)

Figure 14. Test Subject No. 2. (a) Unfiltered Subject as Viewed on the Monitor; (b) Blur Coded Image.

(a) (b)

Figure 15. Test Subject No. 2. (a) Simulated Decoded Image Using One-Channel Decoding; (b) Simulated Decoded Image Using Two-Channel Decoding.

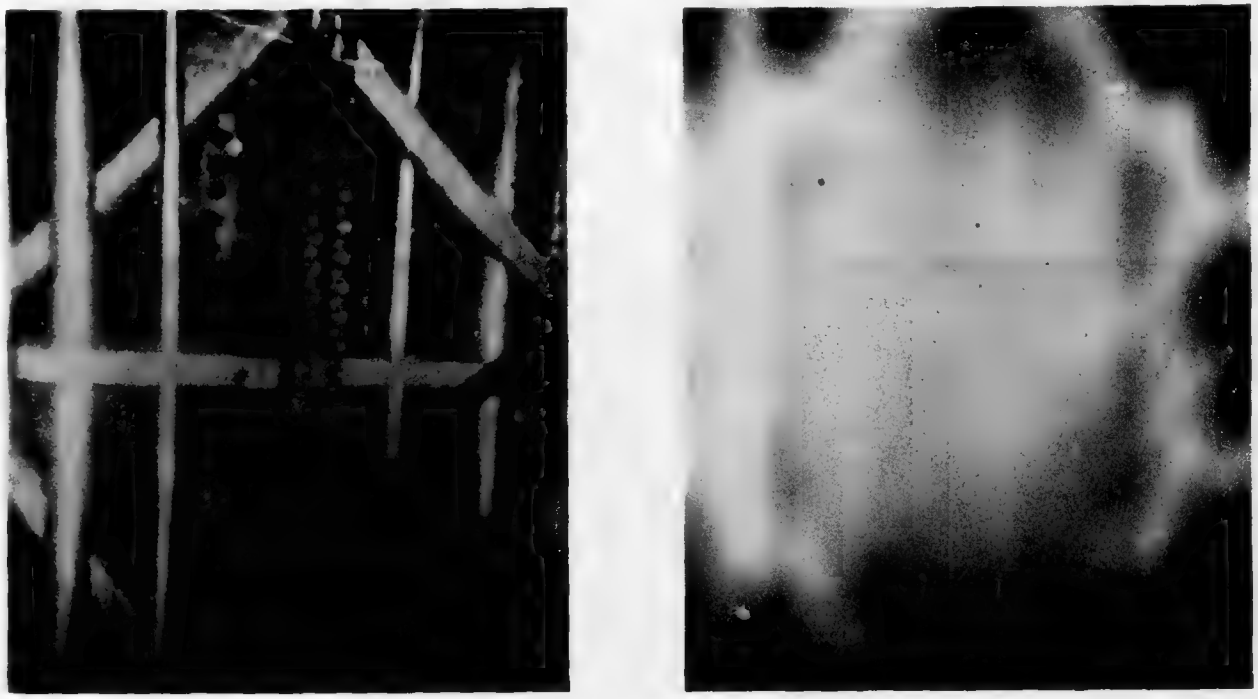

(a) (b)

Figure 16. Test Subject No. 3. (a) Unfiltered Subject as Viewed on the Vidicon Monitor; (b) Blur Coded Image.

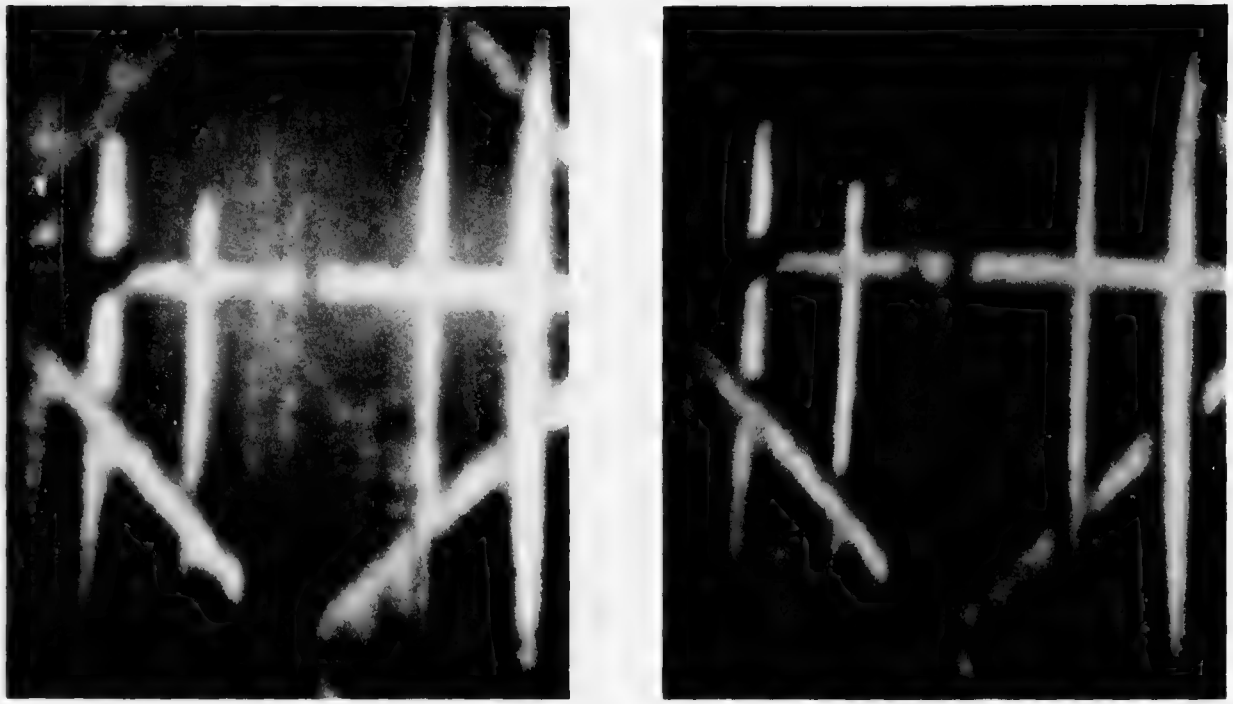

(a) (b)

Figure 17. Test Subject No. 3. (a) Simulated Decoded Image Using One-Channel Decoding; (b) Simulated Decoded Image Using Two-Channel Decoding.

(1) The original unfiltered subject as viewed on the monitor,

(2) A blur-coded photograph,

(3) A simulated decoded image using one-channel coding and decoding, and

(4) A simulated decoding image using two-channel coding and decoding.

The blurred picture was simulated by using incoherent correlation. The blurring is equivalent to convolving the test transparency with a disk 2.2 mm in diameter. This is explained in Appendix II. Comments about the comparison between the coded and decoded image in each case are made below

3.10.1 Test Subject No. 1. (See Figs. 12 and 13). The two-channel scheme shows sharper edges around windows. The general shape of the tower is better defined.

3.10.2 Test Subject No. 2. (See Figs. 14 and 15). In the two-channel decoded image, certain edges of the building facade show that are missing in the one-channel decoded image.

Notice also that some of the window bracing is starting to appear in the two-channel version. There is also better contrast in the water ducts.

3.10.3 Test Subject No. 3. (See Figs. 16 and 17). All of the structural edges and lines are sharper in the two-channel case. The links in the cahin structure are also visible.

3.10.4 General Observations. In all subjects line and edge structure is improved. This agrees well with observations made by Ragnarsson [29] on results using a one-channel filter in deblurring. He discusses the unavoidable "ghost images" around sharp edges. This edge degrading effect is analogous to the ghosts that occur in a modulated pulse train or due to faults in ruled diffraction grating.[53] As seen from Fig. 9(a), the spectrum is modulated by a "circular grating." This grating is not perfect since the line widths and spacings vary. This leads to edge ghosts which are analogous to the ghost sidebands of ruled gratings. It is this effect that can be most effectively removed using multichannel filtering on deblurring.

CHAPTER 4

CONCLUSIONS AND SUGGESTIONS FOR FUTURE RESEARCH

The interesting results in Chapter 3 not only suggest immediate applications, but also offer a basis for further exploration. The conclusions that follow from these results are discussed here. Also, certain ideas that occurred during this research, but not yet pursued, are proposed.

4.1 CONCLUSIONS

A new and novel idea, multichannel image decoding, has been presented. This scheme is quite general and has been tested for the specific case of a blur-coded image. It has been shown (using a graphical analysis) that in theory a two-channel code can provide nearly 37% more information in the frequency plane using an inverse filter with a dynamic range of 100. Furthermore, it is expected from this analysis that the degrading effects due to the information gaps near

nulls in the blur-coded transfer function can be eliminated.

The optical simulation of Chapter 3 shows that the most detrimental effects of the information gaps in blur coding is "ghosting" of edges. Also, it is shown that there is a definite improvement in edge and line structure if two-channel decoding is used instead of the conventional one-channel decoding scheme. It can be expected from these results that multichannel filtering should improve the present "state of the art" in inverse filtering schemes where the coded image has high signal-to-noise ratio in the recording process.

It is also obvious from the results shown that other coding schemes that are similar to blur coding will also show improvement through multichannel decoding. "Similar" means codes that have coding transfer functions with periodic or nearly periodic nulls, such as the coding transfer function for motion blur.

Also it might be noted that the same graphical analysis used in Chapter 3 is also applicable if the transfer function is circularly symmetric or varies in only one direction

in the frequency plane. This represents a small class of functions, but it is an important class in optical applications. Besides extending the analysis to other functions, the user can easily extend it to cover more channels. This requires only the use of more graph overlays. This graphical approach is easy to use and is interactive since it allows the user to see the composite transfer function and make intuitive adjustments.

There are disadvantages in the multichannel decoding. It requires more than one coding channel and hence more recording and information processing. Also, there is no general way to decide the best way to carry out the coding process. Its usefulness will depend on the given situation as to whether it is worth the additional effort.

It can be expected that certain applications can immediately benefit from these results. The particular case of misfocus blurring is applicable to electron micrographs where phase objects are purposely misfocussed to make an intensity recording. Also, in aperture coded imaging where

a circular aperture is used, the same coding transfer function occurs and the analysis of Chapter 3 is applicable.

4.2 SUGGESTIONS

Several interesting ideas have arisen that unfortunately could not be pursued. Hopefully, this work will create enough interest to see that they are carried out. The primary problem with multichannel filtering lies in its implementation.

The easiest technique for applying multichannel filtering involves the use of a digital computer. Each coding channel can be Fourier transformed using a two-dimensional fast Fourier transform algorithm. Then for a given point in the frequency plane, the computer can select which channel optimizes the signal-to-noise ratio. The particular frequency plane point is then decoded using inverse filtering. All this is quite obvious and straightforward; however, it is not obvious how to carry out such a procedure optically. Although it is quite easy to obtain the Fourier transform of any given coded image using a lens, it is not easy to select pieces from each transform

and combine them into a single transform to get a decoded image. In principle, such a process is possible. Each channel could be transformed using a lens; a binary filter in the transform plane could select those parts of the transform for each channel which were important in recovery; then the separate pieces could be brought together using mirrors to form the Fourier transform of an image coded with the composite coding function. The composite inverse filter can be made holographically from each piece of the composite transform using any of the conventional holographic deconvolution techniques.

There are obvious difficulties with this scheme. Each piece in the mosaic forming the composite coding transform must be phase-matched with pieces contiguous to it. This may not be easy if many channels are used. If only two channels are used, then an optical phase shifter in one channel could be adjusted until the best decoded image was observed. With many channels it would be difficult to adjust the phase of each channel independently.

In addition to the problems cited above, the scaling, size, and position of all the filters and the input transparencies are critical. Therefore, it appears that alternate schemes need to be developed. It certainly looks more feasible to record the coded images on the same film and use some scheme to separate them optically, such as grid-coding[54] techniques.

Besides the implementation problems, a great deal more research is needed in creating new coding schemes. There are many transfer functions that can complement each other and improve the overall signal-to-noise ratio. The work here represents only a small effort.

Since the computer can be used directly to implement multichannel decoding, it should be tried as soon as possible on "real world" problems such as improvements on electron micrographs. The additional information certainly appears worth the effort, as shown in the simulation. If such results can be achieved in practice, then an improvement in the resolution of the electron microscope for phase objects is possible.

APPENDIX 1

PRODUCTION OF A TRANSPARENCY WITH AN E-FIELD TRANSMITTANCE PROPORTIONAL TO A GIVEN INTENSITY DISTRIBUTION

Tsujuichi[24] has shown it is possible to record an E-field amplitude transmittance on photographic film that is directly proportional to a given object intensity if the contrast in the recorded object is low. A low contrast object intensity distribution across the x-y plane is described by

$$o(x, y) + a$$

where $o(x, y)$ represents small variations in the recording about a large constant background a. The final recorded intensity transmittance in a photographic positive made from the intensity distribution is T_I, where

$$T_I \propto \left[o(x, y) + a \right]^k,$$

and k is a constant that is equal to the product of the photographic gammas used in making the original negative and the final positive transparency.[42] Note that E-field transmittance

T_E is proportional to the square root of the intensity transmittance.. Therefore,

$$T_E \propto T_I^{\frac{1}{2}}$$

or

$$T_E \propto \left[o(x, y) + a \right]^{k/2} .$$

But using the binomial theorem

$$\left[o(x, y) + a \right]^{k/2} \approx a^{k/2} + \frac{k}{2} o(x, y),$$

then

$$T_E \propto a^{k/2} + \frac{k}{2} o(x, y) .$$

Therefore, T_E is proportional to $o(x, y)$.

APPENDIX II

USING INCOHERENT CONVOLUTION TO CREATE A BLUR-CODED IMAGE

An aperture coded imaging system, as shown in Fig. 18, can be used to create a blur-coded image. Misfocus blur is equivalent to convolution with a circular disk. In Fig. 18 a subject transparency is diffusely illuminated by incoherent light. Any point source on the transparency projects an image of the circular coding aperture. The coding aperture has a diameter D_A, while the projected impulse response on the film has a diameter D_F. From the geometry:

$$D_F = \frac{\ell_1 + \ell_2}{\ell_1} D_A. \qquad \text{(I-1)}$$

Therefore, for a given subject intensity distribution $I(x_1, y_1)$, the projected intensity distribution is † proportional to

---

†The "circ" function is defined as

$$\text{circ}\left(\sqrt{x^2 + y^2}\right) = \begin{cases} 1 \text{ if } \sqrt{x^2 + y^2} \leq 1 \\ 0 \text{ if } \sqrt{x^2 + y^2} > 1 \end{cases}$$

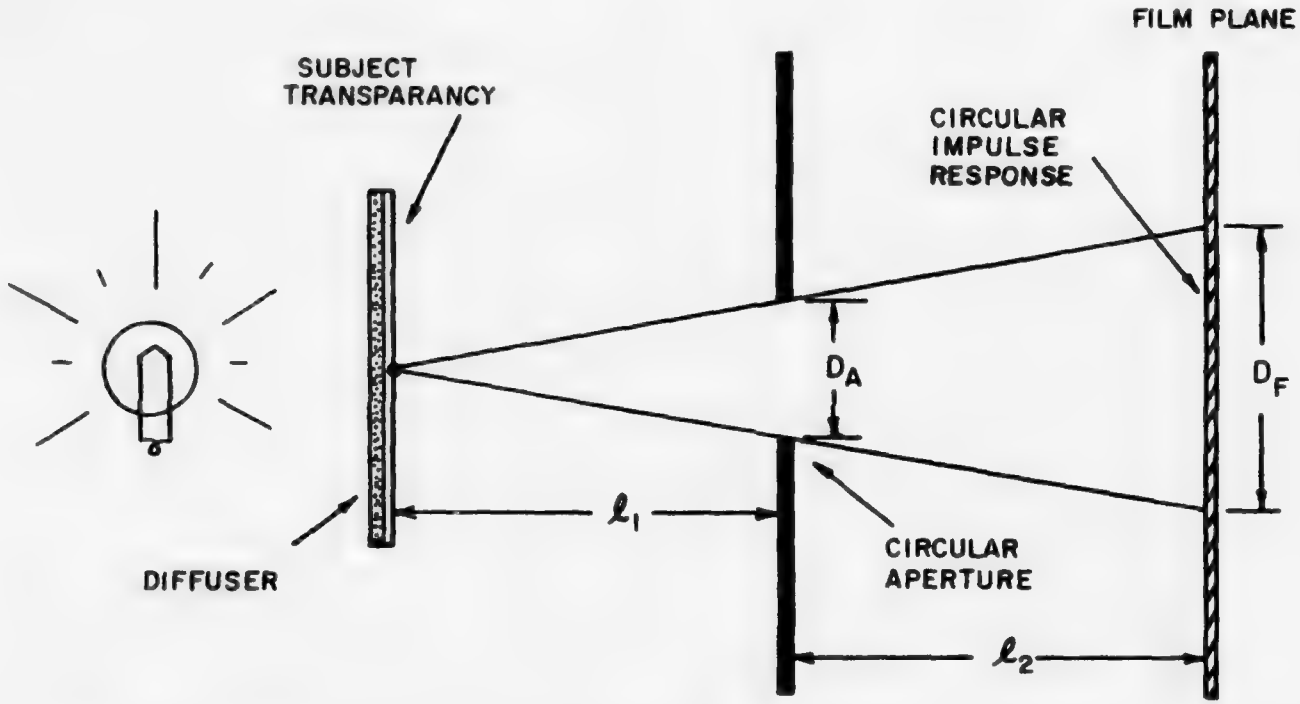

Figure 18. A Point Source on the Subject Transparency Projects a Circular Impulse Response at the Film Plane.

$$I\left(\frac{\ell_1}{\ell_2}\ x_2,\ \frac{\ell_1}{\ell_2}\ Y_2\right) * \text{circ}\left(\frac{2\sqrt{x_2^2 + y_2^2}}{D_F}\right)$$

in the film plane. Note that the projected image I in the convolution is scaled by $\ell_2\ \ell_1$. This can be seen by considering the case for a small value of D_A, then the "circ" function becomes a Dirac δ-function and the system acts as a simple pinhole camera. If the original subject $I(x_1, y_1)$ is to be blurred by coding it with a disk of diameter D_o, then the projected image, in order to have an equivalent amount of blur, must be convolved with

$$\frac{\ell_2}{\ell_1}\ D_o\ ,$$

therefore,

$$D_F = \frac{\ell_2}{\ell_1}\ D_o\ ,$$

but using (I-1) gives

$$D_A = \left(1 + \frac{\ell_1}{\ell_2}\right)\ D_o \qquad \text{(II-2)}$$

Using Eq. (II-2), the correct diameter of the coding aperture can be determined for a projected blurred image if the size disk that the subject transparency is to be convolved with is known

AD-A035 378 TEXAS UNIV AT AUSTIN ELECTRONICS RESEARCH CENTER F/G 9/4
MULTICHANNEL IMAGE DECODING,(U)
JAN 76 J KNOPP, E L HIXSON
UNCLASSIFIED TR-178 F44620-71-C-0091 AFOSR-TR-77-0009 NL

2 OF 2
AD-A
035378

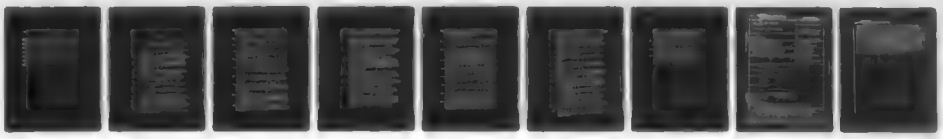

END
DATE
FILMED
3-16-77
NTIS

(i.e., D_o). In Chapter 3, $D_o \cong 2.2$ mm.

The aperture coding operation shown in Fig. 18 was carried out using a photographic enlarger. The enlarging lens was replaced with the correctly scaled circular stop. A negative of one of the test subject transparencies was placed in the enlarger and adjusted for the scale to be used in printing with the enlarging lens. The correctly adjusted stop was then installed and used to obtain an enlarged blur coded image directly on print paper.

REFERENCES

1. Hunt, B. R., "Digital Image Processing," Proceedings of IEEE, Vol. 63, 1975, p. 693.

2. Hsu, M. P., Fourier Analysis, Simon and Schuster, New York, 1970.

3. Bracewell, R. N., The Fourier Transform and Its Applications, McGraw-Hill Book Company, New York, 1965.

4. Lighthill, M. J., Introduction to Fourier Analysis and Generalized Functions, Cambridge University Press, New York, 1960.

5. Papoulis, A., The Fourier Integral and Its Applications, McGraw-Hill Book Company, New York, 1962.

6. Bragg, W. L., "A New Type of X-Ray Microscope," Nature, Vol. 143, 1939, p. 678.

7. Bragg, W. L., "The X-Ray Microscope," Nature, Vol. 149, 1942, p. 470.

8. Gabor, D., "A New Microscope Principle," Nature, Vol. 161, 1948, p. 777.

9. Gabor, D., "Microscopy by Reconstructed Wavefronts," Proceedings of the Royal Society, Vol. A197, 1949, p. 454.

10. Phillips, W. R., and D. McLachlan, Jr., "A Versatile Projector for Assisting in Crystal Structure Determinations," Review of Scientific Instruments, Vol. 25, 1954, p. 123.

11. Rogers, G. L., "The Black and White Hologram," Nature, Vol. 166, 1950, p. 1027.

12. Rogers, G. L., "Gabor Diffraction Microscopy: The Hologram as a Generalized Zone Plate," Nature, Vol. 166, 1950, p. 237.

13. Mertz, L., Transformations in Optics, John Wiley and Sons, Inc., New York, 1965.

14. Young, N. O., "Photography Without Lenses or Mirrors," Sky and Telescope, Vol. 26, 1963, p. 8.

15. Barrett, H. H., and D. T. Wilson, "Fresnel Zone Plate Imaging in Radiology and Nuclear Medicine," Optical Engineering, Vol. 12, 1963, p. 8.

16. Rogers, W. L., I. W. Jones, and W. H. Beierwaltes, "Imaging in Nuclear Medicines with Incoherent Holography," Optical Engineering, Vol. 12, 1973, p. 13.

17. Barrett, H. H., and F. A. Harrigan, "Fresnel Zone Plate Imaging of Gamma Rays," Applied Optics, Vol. 12, 1973, p. 2686.

18. Dicke, R. H., "Scatter Hole Cameras for X-Rays and Gamma Rays," Astro. Phys. Journal, Vol. 153, 1968, p. L101.

19. Groh, G., G. S. Hayat, and G. W. Stroke, "X-Ray and γ-Ray Imaging with Multiple Pinhole Cameras Using a Posteriori Image Synthesis," Applied Optics, Vol. 11, 1972, p. 921.

20. Weiss, H., "Nonredundant Point Distribution for Coded Aperture Imaging with Application to Three-Dimensional On-Line X-Ray Information Retrieval," IEEE Transactions on Computers, Vol. C-24, 1975, p. 391.

21. Goley, M. J. E., "Point Arrays Having Compact, Nonredundant Autocorrelations," Journal of the Optical Society of America, Vol. 61, 1971, p. 273.

22. Wouters, A., K. A. Simon, and J. G. Huschberg, "Direct Method of Decoding Multiple Images," Applied Optics, Vol. 12, 1973, p. 1871.

23. Marechal, A., P. Croce, and K. Dietzel, "Amelioration Du Contraste Des Details Des Images Photographiques Por Filtage Des Frequences Spatiales," Optica Acta, Vol. 5, 1958, p. 256.

24. Tsujuichi, J., "Correction of Optical Images by Compensation of Aberrations and by Spatial Frequency Filtering," in E. Wolf (ed.) Progress in Optics, Vol. II, North-Holland Publishing Company, Amsterdam.

25. Tsujuichi, J., and G. W. Stroke , "Optical Image Deblurring Methods," Proceedings of U.S.-Japan Seminar on Information Processing by Holography, in Barrekette et al (ed.), Applications of Holography, p. 259, Plenum Press, New York.

26. Stroke, G. W., and R. G. Zech, "A Posteriori Image Correcting Deconvolution by Holographic Fourier-Transform Division," Physics Letters, Vol. 25A, 1967, p. 88.

27. Stroke, G. W., "Image Deblurring and Aperture Synthesis Using a Posteriori Processing by Fourier-Transform Holography," Optica Acta, Vol. 16, 1969, p. 401.

28. Stroke, G. W., and M. Halioua, "A New Holographic Image Deblurring Method," Physics Letters, Vol. 29A, 1972, p. 269.

29. Ragnarsson, S. I., "A New Holographic Method of Generating a High Efficiency Extended Range Spatial Filter with Applications to Restoration of Defocussed Images," Physica Scripta, Vol. 2, 1970, p. 2.

30. Tichenor, D. A., "Extended Range Spatial Filters for Image Deblurring," Dissertation at Stanford University in Electrical Engineering, 1973, available from University Microfilms #73-27,128.

31. Harris, Sr., J. L., "Image Evaluation and Restoration," Journal of the Optical Society of America, Vol. 56, 1966, p. 569.

32. Harris, Sr., J. L., "Potential and Limitations of Techniques for Processing Linear Motion Degraded Imagery," in Evaluation of Motion Degraded Images, p. 131, U.S. Government Printing Office, Washington, D.C., 1968.

33. Horner, J. L., "Optical Spatial Filtering with the Least Mean-Square-Error Filter," Journal of the Optical Society of America, Vol. 59, 1969, p. 553.

34. Stockham, T. G., T. M. Cannon, and R. B. Ingebretson, "Blind Deconvolution Through Digital Signal Processing," Proceedings of IEEE, Vol. 63, 1975, p. 678.

35. Sondhi, M. M., "Image Restoration: The Removal of Spatially Invariant Degradation," Proceedings of IEEE, Vol. 60, 1972, p. 842.

36. Huang, T. S., W. F. Schreiber, and O. J. Tretiak, "Image Processing," Proceedings of IEEE, Vol. 59, 1971, p. 1586.

37. Oppenheim, A. V., R. W. Schafer, and T. G. Stockham, "Nonlinear Filtering of Multiplied and Convolved Signals," Proceedings of IEEE, Vol. 56, 1968, p. 1264.

38. Ratcliffe, J. A., "Some Aspects of Scalar Diffraction Theory and Their Application to the Ionosphere," in Reports on Progress in Physics, (A. C. Strickland, ed.) Vol. XIX, p. 188, The Physical Society, London, 1956.

39. Collier, R. J., C. B. Burckhardt, and L. H. Lin, Optical Holography, Academic Press, New York, 1971.

40. Cathey, W. T., Optical Information Processing and Holography, John Wiley and Sons, New York, 1974.

41. Born, M., and E. Wolf, Principles of Optics, Pegamon Press, New York, 1965.

42. Goodman, J. W., Fourier Optics, McGraw-Hill Book Company, New York, 1968.

43. Sommerfield, A., Optics, Academic Press, New York, 1967.

44. Baker, B. B., and E. T. Copson, The Mathematical Theory of Huggens Principle, Clarendon Press, Oxford, England, 1950.

45. Silver, S. S., "Microwave Aperture Antennas and Diffraction Theory, Journal of the Optical Society of America, Vol. 52, 1962, p. 131.

46. Vander Lugt, A., and R. H. Mitchel, "Technique for Measuring Modulation Transfer Functions of Recording Media," Journal of the Optical Society of America, Vol. 57, 1967, p. 372.

47. Kodak Plates and Films for Scientific Photography, Eastman Kodak Company, 19

48. Lash, H., Vector and Tensor Analysis, McGraw-Hill Book Company, New York, 1950.

49. Helstrom, C. W., "Image Restoration by the Method of Least Squares," Journal of the Optical Society of America, Vol. 57, 1967, p. 297.

50. Horner, J. L., "Optical Restoration of Images Blurred by Atmospheric Turbulence Using Optimum Filter Theory," Applied Optics, Vol. 9, 1970, p. 167.

51. Hopkins, H. H., "The Frequency Response of a Defocussed Optical System," Mathematics and Physics Proceedings of the Royal Society, London, Vol. 231A, 1955, p. 91.

52. Private communication from D. H. Williams, Department of Electrical Engineering, The University of Texas at Austin, Austin, Texas.

53. Stuart, R. D., An Introduction to Fourier Analysis, Methuen and Company, Ltd., 1969.

54. Pennington, K. S., P. M. Will, and G. L. Shelton, "Grid Coding: A Technique for Extraction of Differences from Scenes," Optical Communication, Vol. 2, 1970, p. 113.

UNCLASSIFIED

SECURITY CLASSIFICATION OF THIS PAGE (When Data Entered)

REPORT DOCUMENTATION PAGE		READ INSTRUCTIONS BEFORE COMPLETING FORM
1. REPORT NUMBER AFOSR - TR - 77 - 0009	2. GOVT ACCESSION NO.	3. RECIPIENT'S CATALOG NUMBER
4. TITLE (and Subtitle) MULTICHANNEL IMAGE DECODING		5. TYPE OF REPORT & PERIOD COVERED INTERIM 6. PERFORMING ORG. REPORT NUMBER
7. AUTHOR(s) Jerome Knopp Elmer L. Hixson		8. CONTRACT OR GRANT NUMBER(s) Cont. F44620-71-C-0091
9. PERFORMING ORGANIZATION NAME AND ADDRESS Electronics Research Center The University of Texas at Austin Austin, Texas 78712		10. PROGRAM ELEMENT, PROJECT, TASK AREA & WORK UNIT NUMBERS 4751 61102F 681306
11. CONTROLLING OFFICE NAME AND ADDRESS AF Office of Scientific Research (NE) Bolling AFB DC 20332		12. REPORT DATE January 15, 1976 13. NUMBER OF PAGES 95
14. MONITORING AGENCY NAME & ADDRESS(if different from Controlling Office)		15. SECURITY CLASS. (of this report) UNCLASSIFIED 15a. DECLASSIFICATION/DOWNGRADING SCHEDULE

16. DISTRIBUTION STATEMENT (of this Report)

Approved for public release; distribution unlimited.

17. DISTRIBUTION STATEMENT (of the abstract entered in Block 20, if different from Report)

18. SUPPLEMENTARY NOTES

19. KEY WORDS (Continue on reverse side if necessary and identify by block number)

Optical Processing
Decoding
Deblurring
Image Restoration
Multichannel Decoding

20. ABSTRACT (Continue on reverse side if necessary and identify by block number)

Multichannel image decoding is a very general scheme to improve the signal-to-noise ratio in decoding images coded with linear shift invariant codes. It is shown that it can be advantageous to code an image with more than one code. A "composite" inverse filter can then be used in the frequency plane to recover the Fourier transform of the original image. To recover a particular point in the frequency plane, the inverse filter for any one of the coded versions of the

DD FORM 1 JAN 73 1473 EDITION OF 1 NOV 65 IS OBSOLETE

UNCLASSIFIED

SECURITY CLASSIFICATION OF THIS PAGE (When Data Entered)

image, that is any channel, can be used. The channel with the highest signal-to-noise ratio is used to recover the desired point. A particular application of this scheme is examined. A two-channel code is compared with a one-channel code in the frequency domain for the case of misfocus blurring. A graphical analysis is given which compares the distance in the frequency plane up to the first zero in the restored transfer function for one- and two-channel deblurring. Binary plots of the restored transfer functions for a dynamic range of 100 are shown for the two different coding schemes. These plots show that the two-channel code recovers 37% more area in the frequency plane than the one-channel code. This increased area restores information missing near zeros in the one-channel transfer function. An optical simulation was made using the binary plots as frequency plane filters. Using photographs of subjects with a significant amount of line and edge structure, it is shown that the two-channel code results in "sharper" decoded images.